TECHNISCHE UNIVERSITÄT DRESDEN

**Fakultät Maschinenwesen** Institut für Festkörpermechanik

Professur für Numerische und Experimentelle Festkörpermechanik

# Projektarbeit im Fachpraktikum

## Benchmarking and evaluation of plane waves DFT-calculations in pure magnesium in its hexagonal closed packed structure

| | |
|---|---|
| Eingereicht von: | Alexander Rehn |
| Matrikelnummer: | 4799194 |
| Studiengang: | Werkstoffwissenschaft |
| Betreuer: | Dr.-Ing. Gabriel Breuil<br>Dr.-Ing. Eric Breitbarth |
| Betreuender Hochschullehrer: | Prof. Dr.-Ing. habil. Markus Kästner |
| Tag der Einreichung: | 31. März 2024 |

# Problem definition

This work takes place into a research project which aim to characterize the electronic properties of materials by the use of quantum computing. The student's work is focused on getting an accurate DFT level of theory of pure magnesium in its hexagonal closed packed structure. In that regard, he will obtain his results by employing Quantum Espresso as the computational framework. An initial work will be done in order to encompass an exhaustive review of the literature regarding magnesium. This will be coupled with a profound understanding of theoretical principles including plane waves, Density Functional Theory (DFT), pseudopotentials, and their implications on electronic structure calculations. Subsequently, a meticulously benchmarking protocol will be implemented, by considering parameters such as smearing methodologies, pseudopotential selections, k-mesh densities, and cut-off energies. The primary objective is to ascertain the optimal level of theory for accurately modelling magnesium's electronic properties. Following the benchmarking procedures, the acquired data will undergo rigorous comparison with established reference datasets, facilitating a discerning evaluation of computational methodologies efficacy and reliability. Then, in the second part of his master thesis, the student will be focused on using the results he presented in this work in order to perform quantum calculations.

# Abstract

For future quantum computer algorithms for quantum chemistry an ansatz is needed. One possibility to get this ansatz is to use density functional theory (DFT) to calculate a wavefunction which is used as a guess wavefunction to build the ansatz. For a DFT calculation simulation parameters are needed. These are the cutoff energies, the k-mesh and which pseudopotential to use. Furthermore smearing parameters were tested to optimize the calculations. To get a guess wavefunction these simulation parameters must be tested. This is called a benchmark to find a sufficient 'level of theory'.

To evaluate the accuracy of the results of the benchmark a point of reference is needed. In this thesis the lattice parameter of a hexagonal close packed (HCP) magnesium crystal were calculated and compared to reference calculations and experiments.

The level of theory for the different pseudopotentials were ascertained and compared.

# Kurzfassung

Für zukünftige Quantencomputeralgorithmen für Quantenchemie benötigen diese einen 'Ansatz'. Dieser Ansatz kann aus einer Wellenfunktion erzeugt werden. Die Wellenfunktion eines Systems mit Dichte-Funktional-Theorie-Rechnungen (DFT) approximiert werden und wird Startwellenfunktion genannt, weil es nur eine wohlbegründete Vermutung als Startwert für den Quantenalgorithmus ist. Für diese DFT-Rechnungen werden Simulationsparameter benötigt. Diese sind mindestens die 'Cutoff'-Energien, das k-Punkt-Gitter und welches Pseudopotential benutzt werden soll. Zusätzlich wurden unterschiedliche Schmier-Algorithmen getestet um die Rechnungen zu optimieren. Damit ein gute Startwellenfunktion berechnet werden können, müssen diese Parameter getestet werden. Das Testverfahren wird 'benchmarking' genannt und dient dazu die richtige Komplexität der zugrundeliegenden Modelle zu wählen.

Um die Genauigkeit der Ergebnisse bewerten zu können, ist ein Vergleichswert notwendig. In dieser Arbeit wurden die Kristallparameter der Rechnungen mit Referenzrechnungen und -experimenten verglichen am Beispiel eines HDP Magnesiumkristalls.

Es wurden hinreichende Simulationsparameter ermittelt und die unterschiedlichen Pseudopotentiale verglichen.

# Contents

# List of Figures

# List of Tables

# List of Symbols

| **Operators and Notation** | Meaning |
|---|---|
| $\hat{f}^{KS}$ | Kohn-Sham one-electron operator |
| $\hat{H}$ | hamilton operator |

| **Latin Symbols** | Unit | Meaning |
|---|---|---|
| $\boldsymbol{a_1}, \boldsymbol{a_2}, \boldsymbol{a_3}$ | Å | unitcell vectors |
| $A$ | Å | length of unitcell vector $\boldsymbol{a_1}$ and $\boldsymbol{a_2}$ |
| $c$ | - | expansion coefficient of plane wave |
| $C$ | Å | length of unitcell vector $\boldsymbol{a_3}$ |
| $E_\rho$ | eV | Cutoff energy for charge density |
| $E_{wfc}$ | eV | Cutoff energy for plane waves |
| $\boldsymbol{G}$ | $\text{Å}^{-1}$ | wave vector of Kohn-Sham orbitals |
| $h$ | $\text{eV}\,\text{s}$ | Planck constant |
| $\hbar$ | $\text{eV}\,\text{s}$ | reduced Planck constant |
| $k_{max}$ | $\text{Å}^{-1}$ | largest norm of a set of wave vectors |
| $\boldsymbol{k}$ | $\text{Å}^{-1}$ | wave vector of a plane wave |
| $n(\cdot), \tilde{n}(\cdot)$ | - | charge density in real, reciprocal space |
| $p$ | $\text{kg}\,\text{Å}\,\text{s}^{-1}$ | momentum |
| $\boldsymbol{r}$ | Å | position vector in real space |
| $\boldsymbol{T}$ | Å | translation vector |
| $V$ | $\text{Å}^3$ | volume of the unitcell to integrate over |
| $V_{\text{eff}}$ | - | effective potential |

| **Greek Symbols** | Unit | Meaning |
|---|---|---|
| $\varepsilon_l$ | eV | eigenenergy of l$th$ Kohn-Sham-Orbital |
| $\lambda$ | Å | wavelength |
| $\rho_0$ | - | ground state density |
| $\varphi_l$,$\tilde{\varphi}_l$ | - | l$th$ Kohn-Sham-Orbital in real, reciprocal space |
| $\psi_k$ | - | one electron wavefunction |
| $\Psi, \Psi'$ | - | many-body wavefunction |

| **Subscripts** | Meaning |
|---|---|

| | |
|---|---|
| cut | cutoff |
| kin | kinetic |
| max | maximal |
| min | minimal |
| wfc | wavefunction |
| eff | effective |

| **Abbreviations** | Meaning |
|---|---|
| BZ | Brillouin zone |
| DFT | density functional theory |
| GGA | generalized-gradient approximation |
| HCP | hexagonal close packed |
| LCAO | linear combination of atomic orbitals |
| LDA | local density approximation |
| PP | pseudopotential |
| SCF | self consistent field |

# 1 Introduction

Two current topics in science are the fast development of quantum computers [1] and the potential of using hydrogen as energy storage. One problem of the latter is the effect of hydrogen on high-strength metals and alloys called hydrogen-embrittlement [2]. Hydrogen-embrittlement causes metals in hydrogen atmosphere to absorb the hydrogen, which leads to decreasing ductility and embrittlement. To understand the mechanism of hydrogen-embrittlement one can use ab initio calculations to simulate the behaviour of atoms [3]. These calculations are limited by their underlying theory. Our hope is that quantum computing algorithms can shine a light on the mechanisms.

## 1.1 Quantum computing

The research interest in quantum computing algorithms increases due to the ongoing improvement of quantum computers and their performance. The huge investments in research and development in this field is due to the expected "Quantum Advantage" of quantum algorithms. The source of this "Quantum Advantage" lies in the structure of the quantum computer and the use of effects of quantum mechanics to compute problems. [1]

### 1.1.1 Workflow

The idea is to create a workflow which combines the computational efficiency of density functional theory (DFT) with the possibilities of a quantum computer. For the quantum computer calculations an ansatz is needed. This ansatz is created by encoding a guess wavefunction. This guess wavefunction can be computed by DFT. The target of this thesis is to prepare the next thesis where this guess wavefunction is used. One can hope that with a better guess the quantum algorithm can be faster or produce accurate results.

## 1.2 Ab initio calculations

To calculate the guess wavefunction we need a equation which describes the wavefunction of a system. This is the Schrödinger equation [4]. It is not analytically solvable for more than two particles. For solving the Schrödinger equation this problem different methods were found. These methods are ordered by accuracy and computational cost on a 'ladder' [5]. At the bottom is the Hartree-Fock method with the least computational cost but also the smallest accuracy [6]. The next 'rungs' are the different exchange-correlation-functionals for the density functional theory (DFT) [5]. The amount of electrons one can reasonable calculated decreases with every 'rung'. After DFT there are so called 'post Hartree-Fock'-methods. These can only calculate a small amount of electrons i. e. 20 electrons in 20

orbitals for a configuration interaction is a huge accomplishment [7]. This is the reason that in thesis different levels of theory of DFT were tested.

### 1.2.1 DFT

Density functional theory uses different approximations i. e. the Born-Oppenheimer approximation to reduce the many-body Schrödinger equation to many one-electron Schrödinger equations in a external effective potential $V_{\text{eff}}$ which creates the influence of the other electrons. It uses that the electron density $n(\boldsymbol{r})$ is one-to-one relatable to the wavefunction of the system. This method calculates the kinetic and potential energies as accurate as possible but can not calculate the 'exchange-correlation' energies exactly. For these exchange-correlation energies the functionals are used. They differ in what information they use [5]. The local density approximation(LDA) and generalized-gradient approximation(GGA) functionals were used.

### 1.2.2 Quantum Espresso

Quantum Espresso is a software packet which was used to run the DFT calculations in this thesis [8–10]. It uses input files which include the description of the system to simulate and simulation parameters to do different kinds of calculations. These calculate energies, can minimize the forces in a system also called 'relaxation' and can calculate electronic properties like the bandstructure.

## 1.3 System

The studied system is the hexagonal close packed(HCP) magnesium crystal. Magnesium has only 2 electrons in the outermost shell and suffers from hydrogen-embrittlement. Its unitcell contains two atoms and a supercell is shown in .

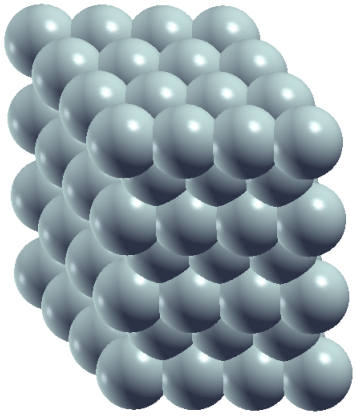

Figure 1.1: The magnesium HCP structure is shown.

## 1.4 Objective

In this essay the objective is to get the appropriate 'level of theory' for a Quantum Espresso calculation to get a guess wavefunction for the quantum algorithms of the next thesis. The 'level of theory' describes a set of input parameter for the simulations which result in a certain accuracy of the simulation. The target is to get the most accurate wavefunction. With a more accurate wavefunction we attain a better ansatz for the quantum algorithm. This results in a hopefully faster quantum calculation and more accurate results. The limiting factor is the computational efficiency the relation between computational time and the accuracy of the result.

# 2 Theory

## 2.1 DFT

DFT stands for density functional theory. Its name comes from the principles of two Hohenberg-Kohn-Theorems. These build the basis for any implementations of DFT. It computes an approximation for the ground state of the system. The ground state is the state with the smallest energy. The ground state is interesting because the ground state is stable and can be used to extrapolate from.

### 2.1.1 Hohenberg-Kohn-Theorems

#### First Theorem

The first Hohenberg-Kohn theorem proofs that the electron density $n(\boldsymbol{r})$ defines uniquely hamilton operator $\hat{H}$ and therefore all properties of the system. They proofed it by proofing that no two different wavefunctions $\Psi, \Psi'$ can have the same $n(\boldsymbol{r})$. [11]

#### Second Theorem

The second Hohenberg-Kohn theorem proofs that the "functional delivers lowest energy if and only if the input density is the true ground state density, $\rho_0$" [11, see p. 36]. This means that one can use the 'variational principle' to find the ground state. The 'variational principle' says that if all allowed densities are computed, the density with the smallest energy is the ground state density with the ground state energy. For DFT it is impossible to test all allowed densities. It is still important because is also means that the density with the least energy of a subset of densities is the best approximation to the ground state of all the densities of the subset.

### 2.1.2 Kohn-Sham-Approach

The Kohn-Sham-Approach tackles the problem of calculating the kinetic energy accurate. It divides the kinetic energy of the electrons in an accurately calculable energy of a non-interacting reference system and a remainder. The method to calculate the non-interacting system accurate and efficient is to introduce the Kohn-Sham-Orbitals and to build them by linear combination of atomic orbitals (LCAO). The remainder consists of correlation energies, self interaction correction, exchange energies and a part of the kinetic energy which is not accurately calculable. The remainder is small in comparison and approximated by the exchange-correlation functional.

#### Kohn-Sham-Orbitals

A Kohn-Sham orbital is a one electron wavefunction $\varphi_i$:

$$\hat{f}^{KS}\varphi_l = \varepsilon_l \varphi_l \tag{2.1}$$

where $\hat{f}^{KS}$ is the Kohn-Sham one electron operator which consists of the kinetic energy, the coulomb interaction between the electron and the nuclei, the electron-electron repulsion and the exchange correlation term. $\varepsilon_i$ is the eigenenergy of this electron.

### 2.1.3 Self consistent field

The self consistent field(SCF) procedure is a iterative algorithm to find a solution for the $\hat{f}^{KS}$ operator and necessary for each DFT calculation.

## 2.2 Unitcell

To describe the system to be simulated we use unitcells and supercells. A unitcell is a volume $V$ defined by three vectors $\boldsymbol{a_1}$,$\boldsymbol{a_2}$,$\boldsymbol{a_3}$:

$$V = \boldsymbol{a_1} \cdot (\boldsymbol{a_2} \times \boldsymbol{a_3}) \tag{2.2}$$

The unitcell of a crystal is defined as smallest volume which when repeated through translation fills space completly and creates the desired crystal (Worch [12]). These translations are defined by the lattice the three vectors $\boldsymbol{a_1}$,$\boldsymbol{a_2}$,$\boldsymbol{a_3}$ create such that:

$$\boldsymbol{T} = N_1\boldsymbol{a_1} + N_2\boldsymbol{a_2} + N_3\boldsymbol{a_3}, N_{1,2,3} \in \mathbb{Z} \tag{2.3}$$

The unitcell consist of $\boldsymbol{a_1}$,$\boldsymbol{a_2}$,$\boldsymbol{a_3}$, the positions and types of the atoms in the unitcell.

A supercell is also defined by three vectors but is a more general formulation. It is a possibility to simulate systems with defects, surfaces or in vacuum. It has not to be the smallest volume, in the opposite way it should be big enough that i. e. defects do not interact with defects in other supercells (Meyer [13]).

### 2.2.1 Plane Wave Basis

One possibility for DFT is to use a plane wave basis set for calculations. A plane wave can be represented by

$$F(\boldsymbol{r}) = e^{\mathrm{i}\boldsymbol{k}\cdot\boldsymbol{r}} \tag{2.4}$$

where $\boldsymbol{r}$ is the position in real space and $\boldsymbol{k}$ is the wave vector. Using plane waves as a basis set is possible possible due to Bloch's theorem [14]. The theorem is valid under the assumption that the crystal behaves like it stretches infinitely in every dimension. This

behaviour is true for undisturbed matrix material. Surfaces and defects can be simulated with the use of supercells.

#### Bloch's Theorem

Bloch's theorem says that the solution $\Psi_{\boldsymbol{k}}$ to the one-particle schrödinger equation in a lattice periodic potential can be represented as a product of a plane wave and a lattice periodic function:

$$\begin{aligned} \Psi_{\boldsymbol{k}}(\boldsymbol{r}) &= u(\boldsymbol{r}) e^{\mathrm{i}\boldsymbol{k}\cdot\boldsymbol{r}} \\ u(\boldsymbol{r}) &= u(\boldsymbol{r}+\boldsymbol{R}) \end{aligned} \tag{2.5}$$

where $u(\boldsymbol{r})$ is the lattice periodic function with the lattice vector $\boldsymbol{R}$.

#### Wave Vector $\boldsymbol{k}$

When the entire system is periodic with translations $\boldsymbol{T}$ like (2.3) the effective potential $V_{\text{eff}}$ of DFT is also periodic:

$$\begin{aligned} \boldsymbol{r} &= \boldsymbol{r} + \boldsymbol{T} \\ V_{\text{eff}}(\boldsymbol{r}) &= V_{\text{eff}}(\boldsymbol{r}+\boldsymbol{T}) \end{aligned} \tag{2.6}$$

A periodic function like $V_{\text{eff}}$ can described by a fourier series:

$$\begin{aligned} V_{\text{eff}}(\boldsymbol{r}) &= \sum_{\boldsymbol{G}} V_{\text{eff}}(\boldsymbol{G}) e^{\mathrm{i}\boldsymbol{G}\cdot\boldsymbol{r}} \\ V_{\text{eff}}(\boldsymbol{G}) &= \frac{1}{V}\int_V V_{\text{eff}}(\boldsymbol{G}) e^{-\mathrm{i}\boldsymbol{G}\cdot\boldsymbol{r}} \mathrm{d}^3\boldsymbol{r} \end{aligned} \tag{2.7}$$

The sum runs over the set of wave vectors $\boldsymbol{G}$ which fulfil the condition $\boldsymbol{G}\cdot\boldsymbol{T} = 2\pi M$ ($M$ is an arbitrary integer)

### 2.2.2 Kohn-Sham-Orbitals

The Kohn-Sham-Orbitals $\varphi_l$ in a plane wave basis are represented by a sum plane waves:

$$\varphi_l(\boldsymbol{r}) = \sum_{|\boldsymbol{G}'|<k_{max}} c(\boldsymbol{G}) \exp(\mathrm{i}\boldsymbol{G}\cdot\boldsymbol{r}) \tag{2.8}$$

The expansion coefficient $c(\boldsymbol{G})$ is stored in the computer for each plane wave.

## 2.3 Calculations

A DFT implementation has different types of calculations it can do. They differ in the calculated property and computational cost. We used so called 'single point' calculations and relaxation calculations.

### 2.3.1 Single-point calculation

A single-point calculation calculates the energies of a given fixed system. It does SCF cycles till the energies are converged. The wavefunctions are calculated.

### 2.3.2 Relaxation calculation

In a relaxation calculation a input geometry is 'relaxed'. Relaxing means minimizing the forces which act on the nuclei and minimizing the total energy. There are different degrees of freedom which can be fixed or relaxed. These degrees of freedom are the positions of the nuclei and the unit cell vectors. In our relaxation calculations all degrees of freedom were relaxed. That means that every atom could move in each direction and the lengths of the unit cell vectors and their angles could change.

It uses a Broyden-Fletcher-Goldfarb-Shanno-algorithm. This is an optimisation algorithm. In DFT-simulations it uses the calculated forces of a single point calculation and changes the unitcell and atomic positions accordingly. Then the new forces of the new geometry are calculated in a single-point calculation and used to change the geometry again, till all forces are below a threshold and the difference of total energy between the steps is below a threshold.

Due to the repeated need of single-point calculations, relaxation calculations take more time to finish.

# 3 Preliminary Studies - The Foundation

For the workflow of the next thesis to start we need a wavefunction which represents the system to simulate. This wavefunction gets encoded by an algorithm. One possibility to get this wavefunction is to use a DFT code to compute it. There are different DFT codes [8–10, 15–17]. They differ in:

- Functionality
  The different implementations include differently complex algorithms to calculate different observables. All implementations calculate the energy of the system and can for example compute a bandstructure. They offer different possibilities to postprocess the calculated data.
- Implementation
  Each code is different and uses their own data structures and file types. There is no standard input or output file for DFT calculations while the content is similar. The implementation can have a impact on computational cost for example by supporting using graphics cards.
- Mathmatical basis
  There are two types of representation of the electron orbitals. Plane waves are just one possibility. The over is to use a more local basis set. These are comprised of often gaussian type orbitals which are localised at nuclei. Abinit [15], Vasp [17] and Quantum Espresso [8–10] use for example plane wave basis sets while Gaussian [16] uses local basis sets.
- Price
  There are open source codes and codes maintained by firms which license them.

## 3.1 Parameter

Cutoff energies, the k-point mesh, the smearing parameters and the pseudopotentials make up the level of theory and will be called simulation parameters. They are the most important parameters which are necessary for each calculation. The smearing parameter are an exception. These smearing parameters are not necessary for each Quantum Espresso calculation but are beneficial for conducting metals.

### 3.1.1 Cutoff energies

The wavefunction cutoff $E_{wfc}$ and the charge density cutoff $E_\rho$ are necessary for each plane wave DFT-calculation. They describe values which determine the amount of plane waves used. For different procedures to calculate different properties different amounts of plane waves are needed. Therefore different cutoff energies are needed.

When using a plane wave basis set, these wavefunctions are approximated by a sum of plane waves. A plane wave is described by its wave vector (see (2.4)). To describe the wavefunction perfectly we need theoretically an infinite number of plane waves. It is computationally not possible to work with an infinite amount of plane waves. That is the reason why a criterion is needed to limit the amount of plane waves. This criterion is the cutoff energy. The kinetic energy of a plane wave is calculated by relating the wavelength of the plane wave to a momentum by the the deBrogli relation:

$$\lambda = \frac{2\pi}{|\boldsymbol{k}|} \tag{3.1}$$

$$\lambda = \frac{h}{p} \tag{3.2}$$

$$p = \frac{h|\boldsymbol{k}|}{2\pi} \tag{3.3}$$

$$p = \hbar|\boldsymbol{k}| \tag{3.4}$$

This momentum combined with the mass of the electron are sufficient to calculate the kinetic energy.

$$E_{kin} = \frac{p^2}{2m} \tag{3.5}$$

$$E_{cut} = \frac{\hbar^2}{2m}|\boldsymbol{k}|^2_{max} \tag{3.6}$$

$$|\boldsymbol{k}|_{max} = \sqrt{\frac{2mE_{cut}}{\hbar^2}} \tag{3.7}$$

It is related to the wave vector $\boldsymbol{k}$ and the mass of the electron $m$. The cutoff energy determines a maximum length of the wave vector $|\boldsymbol{k}|_{max}$ like in equation (3.6) and (3.7) shown. The origin of the idea to limit the wave vector is in the relation between the wave vector and the wavelength $\lambda$ of the plane wave. The wavelength of a plane wave determines the smallest feature it can model. The wavelength is defined by the wave vector as (3.1).

$$\lambda_{min} = \frac{2\pi}{\sqrt{\frac{2mE_{cut}}{\hbar^2}}} \tag{3.8}$$

With this relation we can use a cutoff energy to limit the wavelength of the used plane waves and calculate the smallest $\lambda_{min}$ of the plane waves used with the equation (3.8). We can limit the number of plane waves needed by deciding a smallest feature size which should be modelled.

### Wavefunction cutoff

To calculate the kinetic energy of the electrons in DFT Kohn-Sham orbitals are used. For the calculation of the kinetic energy the cutoff energy is called wavefunction cutoff $E_{wfc}$ or kinetic cutoff. This energy ($E_{wfc}$) describes one part of the accuracy of the approximation of the wavefunction.

### Charge density cutoff

The charge density $n(\boldsymbol{r})$is calculated as the square of the Kohn-Sham-orbitals $\varphi_l$.

$$n(\boldsymbol{r}) = \sum_l \varphi_l^*(\boldsymbol{r})\varphi_l(\boldsymbol{r}) \tag{3.9}$$

Due to computational reasons these equations are calculated in reciprocal space:

$$\tilde{n}(\boldsymbol{k}) = \sum_l \sum_{|\boldsymbol{k'}|<k_{max}} \tilde{\varphi}_l^*(\boldsymbol{k'})\tilde{\varphi}_l(\boldsymbol{k}-\boldsymbol{k'}) \tag{3.10}$$

We see that the product in real space transforms in a convolution in reciprocal space. Also there are non-zero Fourier components up to $2k_{max}$. That is the reason we need a second cutoff energy $E_\rho$ which is at least 4 times as big as $E_{wfc}$. 4 times because the square root of the cutoff energy determines the maximum norm, see equation (3.7) and table 3.1. In this table it is shown that when the cutoff energy is quadrupled the wavelength halves. Furthermore the used cutoffs are shown to get a relation between cutoff and wavelength. Even higher cutoffs should be tested to be certain. The number of plane waves for charge density calculations is determined by the charge density cutoff energy $E_\rho$.

## 3.1.2 k-Point Mesh

To sample the first Brillouin zone we need a so called k-mesh. The k-mesh defines how accurate the Brillouin zone is sampled and with which symmetries. The k-mesh consists of a grid k-points mostly defined by the amount of k-points in each direction of the coordinate system. The last defining parameter of the k-mesh is if the k-mesh is shifted in relation to

Table 3.1: This table shows the relation between common $E_{cut}$ and their $\lambda_{min}$.

| $E_{cut}$ | $\lambda_{min}$ |
|---|---|
| 10 Ry | 1.051 Å |
| 13 Ry | 0.922 Å |
| 52 Ry | 0.461 Å |
| 100 Ry | 0.332 Å |
| 400 Ry | 0.166 Å |

the coordinate origin. The coordinate origin is called the Γ -Point. Only the first Brillouin zone(BZ) has to be sampled because all other are symmetric to the first. Because this Brillouin zone is in the reciprocal space the amount of k-points along each axis should be inversely proportional to the length of the unitcell vectors.

The k-mesh is generated in a MONKHORST-grid [18]. It has always the same symmetries as the unitcell. The Monkhorst-grid is generated out of the density of k-points along each reciprocal direction. It is written like $k_x \times k_y \times k_z$ where $k_x, k_y, k_z$ are the amount of k-points in the according direction in the first BZ.

### 3.1.3 Smearing

One optimisation possibility for conducting metals is to introduce smearing. Smearing describes the behaviour of occupation near the Fermi-level. It introduces a broadening of discrete levels. There are different methods to introduce this broadening like 'Fermi', 'Gaussian', 'Methfessel-Paxton' and 'Marzari-Vanderbilt'.

### 3.1.4 Pseudopotentials (PP)

The last important parameter to consider is the pseudopotential which should be used. It describes the behaviour of inner electrons. The wavefunction of these inner electrons rapidly oscillates around the core. To replicate this behaviour we would need a very high wavefunction cutoff energy. Even with this high cutoff we would not get any important information because in our system the inner electrons have not got a great effect on the behaviour of the system. That is why we introduce PPs which describe a smoother substitution for these electrons. There is a need for different pseudopotentials for each element in the system because the inner electrons behave differently. Different pseudopotentials substitute different amounts of inner electrons i. e. there are PPs which treat all but the outer shell as inner electrons and some which treat all but the outer two shells as inner electrons.

The pseudopotentials can be sorted in 3 different ways:

- **Functional** They can be sorted by the functional used into LDA and GGA. For GGA the PBE and PBEsol functional were compared.
- **Active electrons** They can be sorted by how many electrons they actively calculate. These pseudopotentials can be sorted into the $2e^-$ and $10e^-$ group. This LDA functional calculates $10e^-$.
- **Pseudopotential type** They can be sorted which type they have. These pseudopotentials can be sorted into PAW and US pseudopotentials. A PAW LDA was used.

## 3.2 Benchmark

One method to reach the objective of attaining the 'level of theory' is a so called benchmark. For that we have to test and optimize the simulation parameters. It is necessary to optimize the testing procedure because there are to many combinations of parameter values to test all of them. If 5 wavefunction cutoffs, 5 charge density cutoffs, 3 smearing methods each with 5 parameter, 20 different k-meshes and 7 PPs are considered, 52500 calculations would be necessary to test each combination. This is not efficient nor feasible. Furthermore it would be common that new values of parameters have to be considered to confirm some results, which would grow this number enormously. That is why we benchmark the simulation parameter. This means that each parameter is tested as separately as possible. For example the k-mesh can be tested separately from the cutoff energies and the smearing parameter. In the opposite way each of these three parameters has to be optimized for each different pseudopotential. This way we get a 'level of theory' for each pseudopotential. Testing is the variation of one parameter while fixing the rest of the parameter and then comparing and interpreting the results. The goal of the benchmark is the convergence (see 3.3) of the simulation parameters.

## 3.3 Convergence

For each of the these parameters we seek a value at which the calculation is 'converged'. Convergence is defined by two aspects. The first is the accuracy, the ability to calculate exact values of observables of the systems. The second aspect is the stability, the ability to find the exact value reliable. A stable calculation means that the result is as good as possible independently of small changes in the starting parameters. We will discuss the accuracy, the stability and criteria for them:

### 3.3.1 Accuracy

Accuracy is a multi layered concept. It describes the deviation from some exact value. This exact value is not accessible. The target is to get as close as possible to this exact value, to get the deviation as small as possible and to know how big or the deviation could be. Experiments as well as simulation suffer from deviations and it is important to know what the reasons are and how it impacts the interpretability of the results. The first aspect is to reach an accurate enough physical description with the simulation that calculated results are meaningful. From a meaningful result one can make good predictions. A model can not describe exactly the behaviour of the systems due to approximations which are necessary in order to tackle computational challenges. The target is that the description is sufficiently accurate that the calculated properties can be used for the cause they are simulated for.

### 3.3.2 Stability

The second aspect is stability. To simulate a geometry the SCF-calculations has to find a stable solution. That means that the difference of two consecutive steps of this iterative algorithm has to be under a certain threshold. This is in our system achievable with recommendations of the pseudopotentials.

To relax a geometry many single point calculation have to be converged. Stability in this context means that independently of small variations in the starting parameters, the relaxation algorithm must still calculate the relaxed geometry. Small variations are changes of the positions of the nuclei. This is the requirement to make predictions for unknown systems. It can be tested by simulation of known systems and comparison with their reference values.

### 3.3.3 Criteria

To decide if and when the simulation is converged is difficult. One possibility is to compare calculated properties to reference values like Yin et al. [19]. They compared experimental values to their calculated lattice constants and elestic constants of hcp metals.

#### Reference values

There are different properties, i. e. lattice parameter, band gap and spectra, one can measure experimentally and calculate in simulations. These are mandatory to evaluate the accuracy of the simulation. One example we use in this work are crystal lattice parameters which can be measured by x-ray crystallography like Barrett and Massalski [20] did. These literature lattice parameters ($A = 3.186\,\text{Å}, C = 5.174\,\text{Å}$) can be compared to results of relaxation calculations. The literature values are at 4 K and the difference to 0 K is in the magnitude of 0.0001 Å and therefore insignificant. Another possibility is to get reference values from other simulations like Yin et al. [19]. To get relaxed lattice parameters we need relaxation calculations, which are much more computational expensive than single-point calculations. To reduce the amount of relaxation calculations we can use single-point calculations to estimate good starting simulation parameters for the relaxation calculations.

#### single-point calculations estimations

Single-point calculations are less computational expensive then relaxation calculations. That is the reason for starting with single-point calculations to benchmark simulation parameters. The output of a single-point calculation does not include relaxed lattice parameters. It outputs different energy values like the total energy $E_{\text{tot}}$ or the bandstructure of the system. We use the total energy as convergence criterion.

Only in comparison the difference between two values of a simulation parameter becomes visible and measurable. The path to a good estimation lies in varying simulation parameter

to evaluate the impact the variation has. One calculated property is the total energy $E_{\text{tot}}$. It is the the sum of all calculated energies in the model. A geometry of atoms with a lower total energy is more stable then a geometry with a higher $E_{\text{tot}}$. In the benchmark we search the simulation parameters with the lowest $E_{\text{tot}}$. Only the lowest $E_{\text{tot}}$ is not an proof of superiority over other models. There are cases were an insufficiently accurate model calculates a lower $E_{\text{tot}}$. The total energy and the circumstances which lead to it have to be interpreted to use it as an indicator. One point of reference is the 'chemical accuracy' of $1\,\text{kJ}\,\text{mol}^{-1}$ targeted by nobel laureate Pople [21]. For a system of 2 atoms it is an equivalent of 0.021 eV per 2 atoms. One has to be careful because this is only for thermodynamic calculations and not electronic calculations. If two models or more differ only in this order of energy the thermodynamic properties should be converged.

### Relaxation calculations

With the starting parameters from the single-point calculation estimations the optimization calculations searches minima. Only if these minima exist can the algorithm find them. This makes the choice of the sufficient simulation parameter important. Optimization calculations search for optimal lattice parameter which we can compare to experiments [20] or other simulation i. e. Yin et al. [19] . For our HCP structure in magnesium we have two defining lattice parameter. The length of the unitcell in x-direction $A$ and the length of the unitcell in z-direction $C$. The relation between these lengths represented by $C/A$ is considered as well. This convolution has information on the shape of the unitcell.

Other calculations could be done to get properties with reference values, like electronic structure calculations, pressure calculations and cohesive energy calculations [22]. There was not enough time to go into detail with these reference properties.

**outputs of relaxation calculations** After a relaxation calculation finished, it outputs the relaxed lattice parameters and atomic positions. In this system the relative position of the atoms did not change because the atoms are in a HCP lattice and already at the optimal position. Even the angles could change but they are also already optimal and did not change. Only the length of the unitcell vectors and the energies did change. To reproduce the calculations of Yin [19] a calculation with the same simulation parameters was done (see '$36 \times 36 \times 19$ k-mesh' in figure 3.5).

### Limits

When the target is to reach the best description of reality raising the accuracy of the simulation would be a reasonable path of accomplishing it. The problem with raising the accuracy is one raises the resources required to compute the simulation. At a certain point there are not enough resources to compute the simulation and often before that there is point where

the raise in accuracy of the simulation is in no relation to the raise of accuracy of the results if any. Therefore we are searching for the parameter set with lowest computational cost but still sufficiently accurate that the results are satisfactory.

## 3.4 Benchmark results

### 3.4.1 Cutoff energies

The first simulation parameters to be benchmarked are the two cutoff parameters. For each pseudopotential and without knowledge of the converged k-point mesh a number of single point calculations were done. Then the total energy is compared to find a suitable value. The results are calculated with an educated guess for the other simulation parameters (Methfessel-Paxton smearing with $E_{\text{degauss}}$= 0.03 Ry;8x8x8 k-mesh) from not included test calculations.

In diagram 3.1 the result of the cutoff benchmark of PBE PAW $2e^-$is shown. The y-axis shows the total energy of the system. The values of $E_{\text{tot}}$ range from $-914.7575\,\text{eV}$ to $-914.748\,\text{eV}$. The difference between the different simulation parameter is only 9.5 meV. This is the reason the y-axis is shifted by by $-914.7\,\text{eV}$ and shown in $meV$. The x-axis shows $E_\rho$ which has to be optimized for each tested $E_{wfc}$. The lower bound of $E_{wfc}$ was set at the lowest recommendation for the pseudopotentials of 13 Ry. Every pseudopotential has its own recommendation. Only combinations of $E_{wfc}$ and $E_\rho$ should be tried were $E_\rho$ is four times as big as $E_{wfc}$, as per the rule introduced in section 3.1.1. The different $E_{wfc}$ are shown as different data series. In (b) the range from $-57.6\,\text{meV}$ to $-57.4\,\text{meV}$ is enhanced because the energy difference between 13 Ry and 40 Ry as $E_{wfc}$ is clearly visible in (a), while the difference between 40 and 100 Ry is minimal.

Generally the total energy stays constant for the tested $E_\rho$ with the exception of the first value $E_\rho = 54\,\text{Ry}$ for $E_{wfc} = 13\,\text{Ry}$ and $40\,\text{Ry}$. The figure 3.1 also shows that for increasing $E_{wfc}$ the calculated total energy falls monotonously until the wavefunction cutoff reaches 80 Ry where the total energy increases the first time. This change in energy difference is an indicator for convergence.

To decide which cutoff energies are sufficient we can evaluate the change of $E_{\text{tot}}$.**The important criteria is the order of magnitude of the change in total energy between different cutoff energies.** The difference between the highest and lowest total energy is only 9.5 meV.

For $E_\rho$ a value of 160 Ry would be sufficient because the total energy does not change significantly after this value. The minimal energy increase at $E_{wfc} = 80\,\text{Ry}$ is an indicator that the description gets better until a plateau is reached at value just below $E_{wfc} = 80\,\text{Ry}$. For these wavefunction cutoffs a charge density cutoff of at least $4E_{wfc} = 320\,\text{Ry}$ should

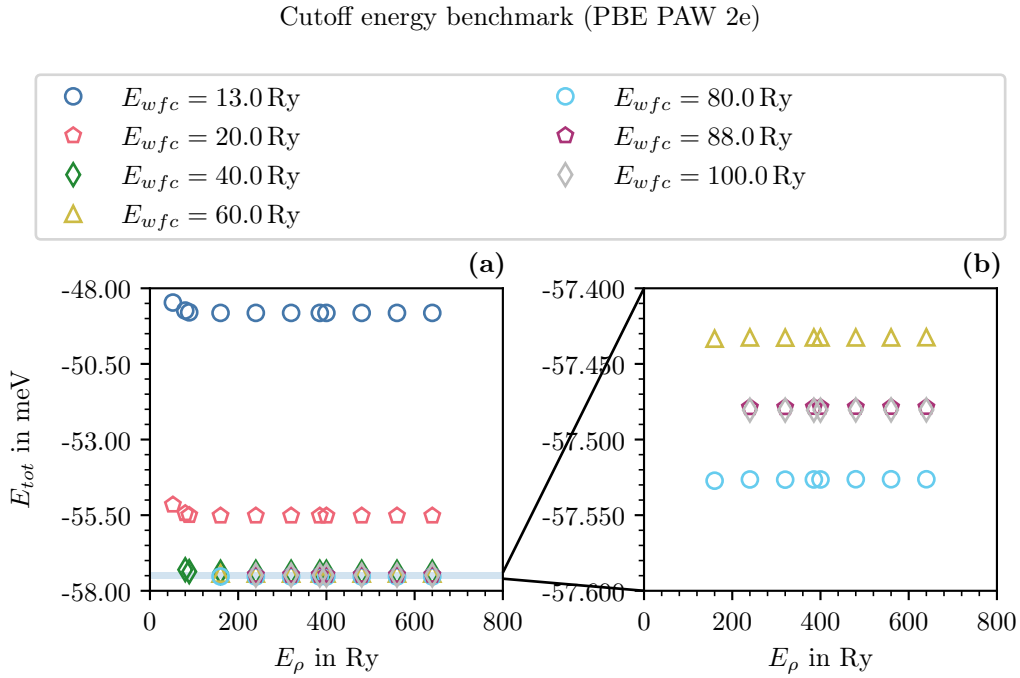


Figure 3.1: Cutoff energy Benchmark: The total energy $E_{\mathrm{tot}}$ of a two magnesium atoms system is depicted over the charge density cutoff $E_\rho$. $E_{\mathrm{tot}}$ is shifted by $-914.7\,\mathrm{eV}$. In (a) the $E_{\mathrm{tot}}$-range from $-58\,\mathrm{meV}$ to $-48\,\mathrm{meV}$ is shown. In (b) the range from $-57.6\,\mathrm{meV}$ to $-57.4\,\mathrm{meV}$ is enhanced. The single-point calculations were done with with following parameters: $A = 3.2\,\mathrm{nm}; C = 5.226\,\mathrm{nm}$; Methfessel-Paxton smearing with $E_{\mathrm{degauss}}$= 0.03 Ry;8x8x8 k-mesh, PBE PAW $2e^-$pseudopotential

be chosen. For this pseudopotential with this k-mesh there would be two possibilities to choose the cutoff energies. If speed is a important aspect and the model should be on only be accurate for thermodynamic calculations a pair of cutoffs of $E_{wfc} = 13\,\mathrm{Ry}; E_\rho = 160\,\mathrm{Ry}$ should be chosen. When the target is to get the best possible result according to the total energy a pair of cutoff energies of $E_{wfc} = 80\,\mathrm{Ry}; E_\rho = 320\,\mathrm{Ry}$ should be chosen.

**Other Pseudopotentials** In the benchmarks of the other pseudopotentials the PP with the highest required cutoffs is the PBEsol PAW $10e^-$PP shown in figure 3.2. In this figure the total energy is shown in **eV** not meV because it shows the range from $-3823.789\,\mathrm{eV}$ to $-3536.000\,\mathrm{eV}$. The y-axis is shifted by $-3500\,\mathrm{eV}$ and in (b) the range from $-323.9\,\mathrm{eV}$ to $-323.6\,\mathrm{eV}$ is enhanced. The same $E_{wfc}$ as in figure 3.1 are shown as data series and the x-axis are the same $E_\rho$.

After $E_\rho$ reaches values above 240 Ry $E_{\mathrm{tot}}$ is constant in our accuracy. With this PP the $E_{\mathrm{tot}}$ is smaller for $E_\rho < 240\,\mathrm{Ry}$. The total energy falls monotonously with increasing wavefunction

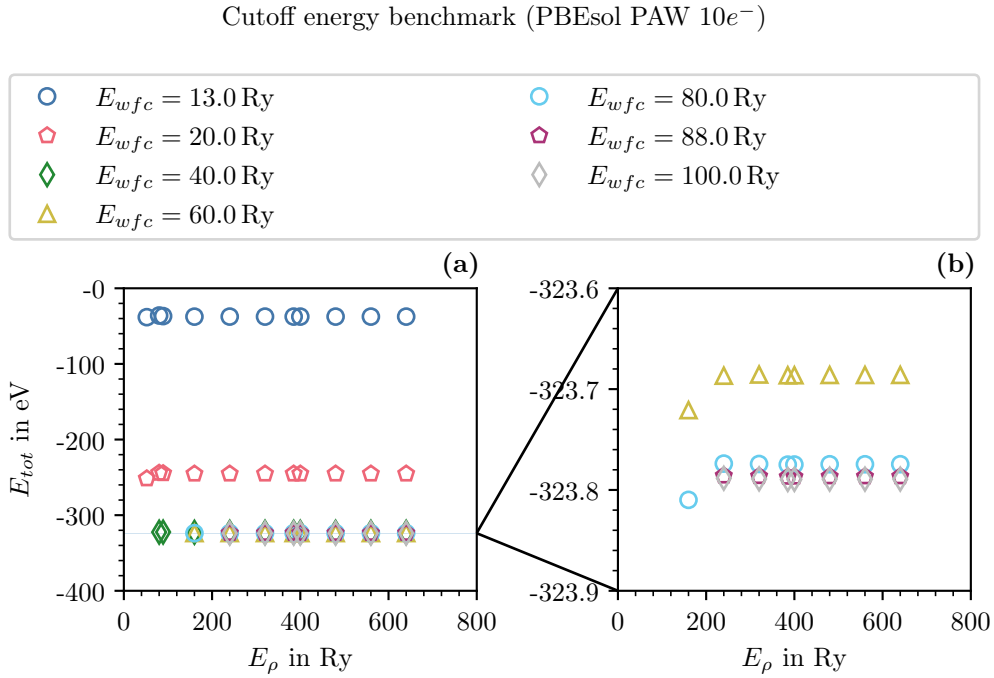


Figure 3.2: Cutoff energy Benchmark: The total energy $E_{\mathrm{tot}}$ of a two magnesium atoms system is depicted over the charge density cutoff $E_\rho$. $E_{\mathrm{tot}}$ is shifted by $-3500\,\mathrm{eV}$. In (a) the $E_{\mathrm{tot}}$-range from $-400\,\mathrm{eV}$ to $0\,\mathrm{eV}$ is shown. In (b) the range from $-323.9\,\mathrm{eV}$ to $-323.6\,\mathrm{eV}$ is enhanced. The single-point calculations were done with with following parameters: $A = 3.2\,\mathrm{nm}; C = 5.226\,\mathrm{nm}$; Methfessel-Paxton smearing with $E_{\mathrm{degauss}}$= $0.03\,\mathrm{Ry}$;$8 \times 8 \times 8$ shifted k-mesh, PBEsol PAW 10$e^-$pseudopotential

cutoff. A $E_{wfc}$ of 20 Ry is insufficient for this PP as seen by the difference in $E_{\mathrm{tot}}$ of over 50 eV between the wavefunction cutoffs of 20 Ry and 40 Ry. Only when reaching a wavefunction cutoff of 100 Ry the difference between 88 Ry and 100 Ry in the magnitude of 1 meV.

That is the reason that for **all following calculations** $E_{wfc} = 100\,\mathrm{Ry}; E_\rho = 400\,\mathrm{Ry}$ **are used** as cutoff energies for all pseudopotentials. With that the accuracy of the results of the different PPs is more comparable in regard of computational cost, because the plane wave accuracy is equal for all different pseudopotentials.

At low charge density cutoffs below $4E_{wfc}$ are outlier of the total energy. They seem more stable energetically but are not a good representation of the system. They show the necessity of the derived $4E_{wfc}$ rule.

### 3.4.2 Smearing

After determining sufficient cutoffs the smearing parameters are benchmarked. These define the behaviour of occupation near the Fermi-level. It is benchmarked by fixing the other

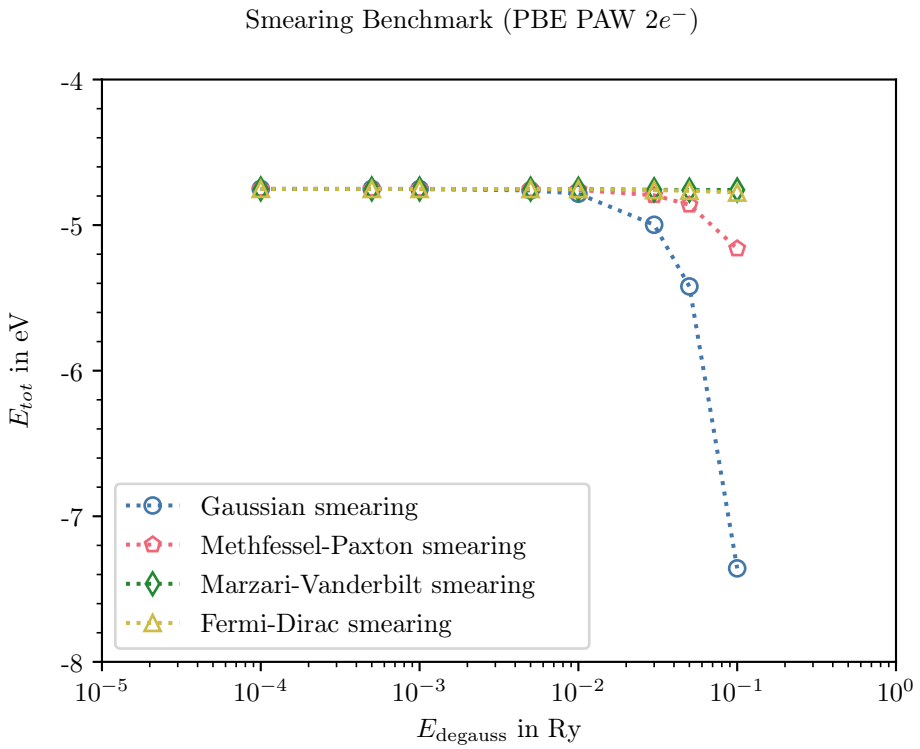


Figure 3.3: Smearing Benchmark: The total energy $E_{\text{tot}}$ of a two magnesium atoms system is depicted over $E_{\text{degauss}}$. $E_{\text{tot}}$ is shifted by $-910\,\text{eV}$. The single-point calculations were done with with following parameters: $A = 3.2\,\text{nm}; C = 5.226\,\text{nm}; E_{wfc} = 100\,\text{Ry}; E_{\rho} = 400\,\text{Ry}$; $8 \times 8 \times 8$ shifted k-mesh, PBE PAW $2e^-$pseudopotential

simulation parameters to following values: $E_{wfc} = 100\,\text{Ry}; E_{\rho} = 400\,\text{Ry}$; $8 \times 8 \times 8$ shifted k-mesh. Then the smearing algorithm is varied and the $E_{\text{degauss}}$-value is changed from 0.0001 Ry to 0.1 Ry. The results with the PBE PAW $2e^-$pseudopotential are shown in figure 3.3. The total energy in eV is plotted over the logarithmic x-axis of $E_{\text{degauss}}$in Ry. The four different algorithm are shown as different series over the logarithmic x-axis.

The total energy changes very little for Marzari-Vanderbilt and Fermi-Dirac smearing, while for Gaussian and Methfessel-Paxton smearing the energy changes by more than 0.5 eV from $E_{\text{degauss}}$= 0.0001 Ry to 0.1 Ry. At high $E_{\text{degauss}}$values the total energy falls.

In the case of cutoff energies and k-mesh a minimal stable total energy is a good benchmark criterium. In the case of smearing a small $E_{\text{degauss}}$with little to no change to the total energy is the target, because it changes the behaviour of the electrons near the fermi level in way that is not representative of the simulated system. That is the reason values of $E_{\text{degauss}}$over 0.03 Ry for Methfessel-Paxton smearing and 0.01 for Gaussian smearing should not be chosen.

In this system we chose for all pseudopotentials 0.03 Ry **for Methfessel-Paxton** smearing because it is a so called 'cold smearing' which does not influence the electrons that significant

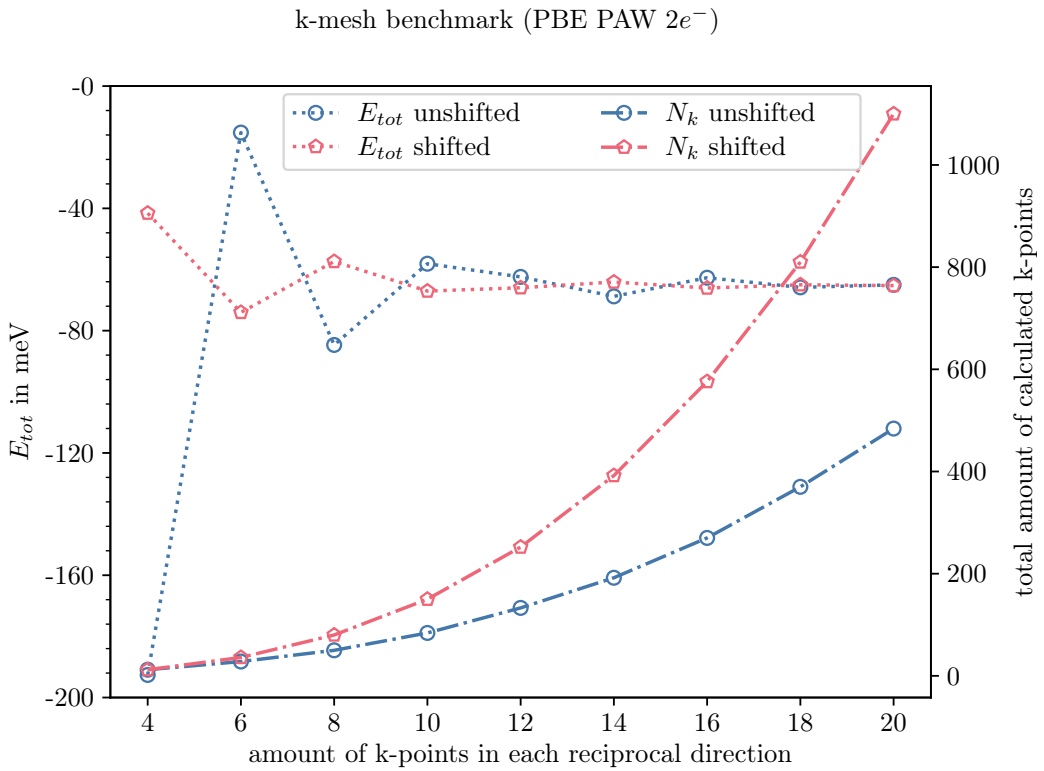


Figure 3.4: k-mesh Benchmark: The total energy $E_{\text{tot}}$ of a two magnesium atoms system and the total amount of calculated k-points is depicted over the used k-mesh in the form of $k_x \times k_y \times k_z$. $E_{\text{tot}}$ is shifted by $-914.7\,\text{eV}$. The single-point calculations were done with with following parameters: $A = 3.2\,\text{nm}$; $C = 5.226\,\text{nm}$; $E_{wfc} = 100\,\text{Ry}$; $E_\rho = 400\,\text{Ry}$; Methfessel-Paxton smearing with $degauss = 0.03\,\text{Ry}$; PBE PAW $2e^-$pseudopotential

(see Marzari [23]). 0.03 Ry are chosen because it is a common value in DFT-calculations and Yin et. al. [19] used a similar value (0.02 Ry).

### 3.4.3 k-Mesh

The k-mesh has two aspects which have to be optimized. The amount of k-points and their placement.

In figure 3.4 the results of the k-mesh benchmark are shown. With the determined simulation parameters from the cutoff and smearing benchmark the results of the PBE PAW $2e^-$pseudopotential are shown. The x-axis shows the amount of k-points in each reciprocal direction of the Monkhorst-Pack k-mesh. The y-axis on the left shows the total energy shifted by $-914.7\,\text{eV}$ for the shifted and unshifted k-meshes for the dotted line. The y-axis on the right shows the total amount of calculated k-points of the calculations. The amounts are shown by the dot-dashed lines in the diagram.

An oscillating behaviour of the total energy is shown with a decreasing amplitude from hundreds of meV to 1 meV. The amplitude in the total energy is smaller when using the shifted mesh. At 18 k-points in each direction the unshifted mesh calculates results in the same magnitude as the shifted one with half as much calculated k-points.

The total amount of calculated k-points rises cubically for the 3 dimensions. The calculated amount starts equal for shifted and unshifted at 12 k-points for a $4 \times 4 \times 4$ k-mesh, but increases faster for the shifted mesh to 1100 calculated k-points in a $20 \times 20 \times 20$ mesh, while the unshifted k-mesh calculated only 484 k-points in a $20 \times 20 \times 20$ mesh.

**Amount of k-points (energy)** In figure 3.4 it is visible, that after a density of 12 k-points the total energy deviates less then 21 meV. We can conclude that the used $8 \times 8 \times 8$ k-mesh is not accurate enough and should use at least a $12 \times 12 \times 12$. It is for every PP the same energy difference between the k-meshes only shifted by a constant energy related to the amounts of electrons the PP calculates.

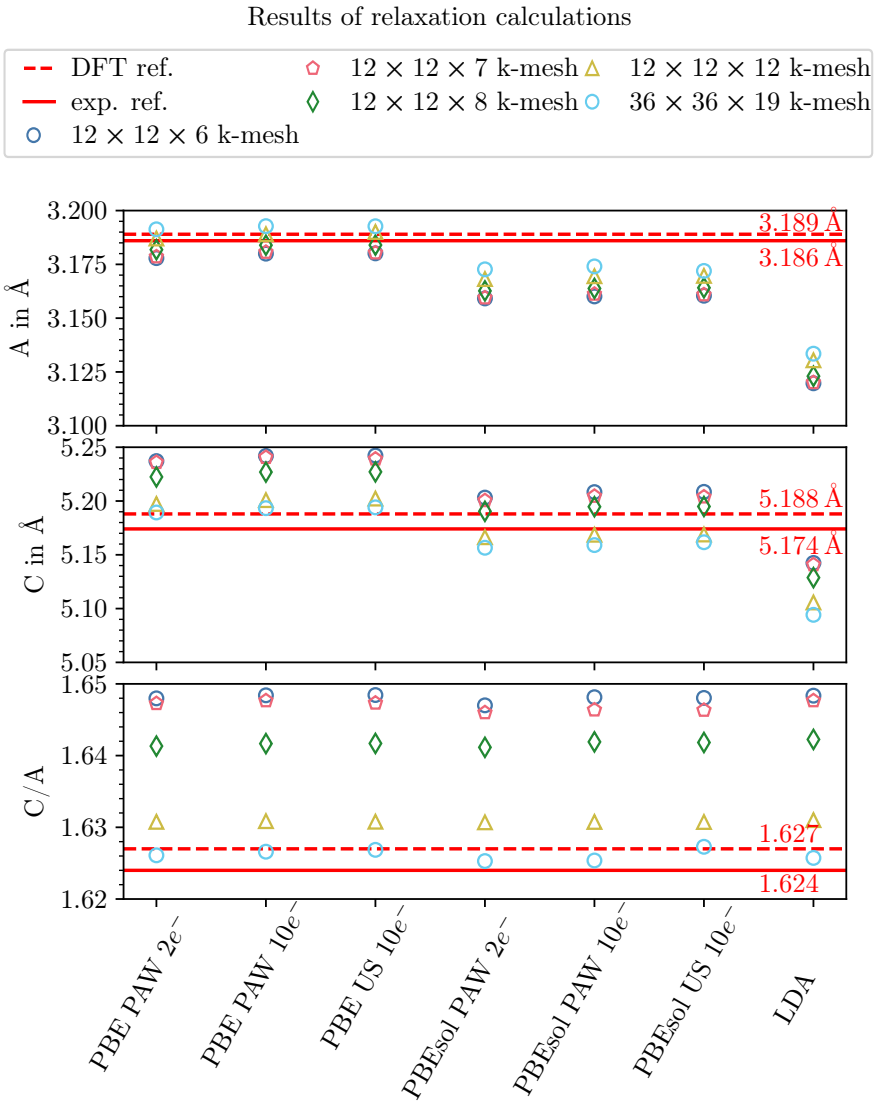


Figure 3.5: k-mesh Benchmark: The lattice parameters $A$ and $C$ of the two magnesium atoms system is depicted over the used k-mesh. The exp. reference is the adjusted value of Barrett [20]. The DFT ref. is from Yin et. al. [19]. The relaxation calculations were done with with following starting parameters: $A = 3.1\,\text{Å}; C = 5.063\,\text{Å}; E_{wfc} = 100\,\text{Ry}; E_{\rho} = 400\,\text{Ry}$; Methfessel-Paxton smearing with $degauss = 0.03\,\text{Ry}$; BFGS algorithm

## 3.5 Relaxation calculation results

After setting minimal values for cutoffs, smearing and k-mesh with the benchmark the second type of calculations were started.

### 3.5.1 Target

After the benchmark is done, the more computationally expensive relaxation calculations are started. These are to ascertain the sufficient k-mesh and to compare the pseudopotentials among each other. It is to test the simulation against reference values to be able to determine the accuracy of the results and the algorithms. To get values which can be compared to the reference values relaxation calculations were needed. Furthermore the guideline that the amount of k-points along the reciprocal directions should be inversely proportional to the length of the according unitcell vector was tested.

### 3.5.2 Starting parameters relaxation calculation

The relaxation calculations started with a non-optimal starting geometry of $A = 3.1\,\text{Å}$ and $C = 5.063\,\text{Å}(C/A = 1.633)$. The starting $C/A$ is the mathematical optimal ratio of a HCP lattice of perfect spheres. The reason for imperfect starting geometry this is to test the ability of the simulation to calculate a good minima. If the starting geometry was optimal we would not know if the algorithm can work to find minima of unknown systems which do not start with optimal starting geometry. A good result of the algorithm in the test system does not mean it works in unknown systems. But if it did not work in the test system it is even more unlikely that it produces good results in more complex cases.

### 3.5.3 Results

In figure 3.5 all the results of the relaxation calculations are shown. In the top diagram the lattice parameter A is shown which is always equal to B. Below the lattice parameter C for the z-direction is shown. In the bottom diagram the ratio $\frac{C}{A}$ is shown. $\frac{C}{A}$ is a ratio which gives insight to the calculated shape of the unitcell. The results are plotted over the used pseudopotential. The different data series are for different used k-meshes. Also the the experimental [20] and DFT [19] reference are shown as full or dashed line in each diagram.

The lattice parameter A increases with the k-point density and in case of PBE PAW $2e^-$, PBE PAW $10e^-$and PBE US $10e^-$overshoots the experimental reference of 3.186 Å. The PBEsol pseudopotentials calculated $A \approx 3.17\,\text{Å}$ and the LDA pseudopotential calculates only $A \approx 3.13\,\text{Å}$.

The lattice parameter C decreases with the k-point density and in case of PBEsol PAW $2e^-$, PBEsol PAW $10e^-$and PBEsol US $10e^-$overshoots the experimental reference of 5.174 Å.

The LDA pseudopotential calculates lengths below the experimental reference and gets even smaller when the k-density is increased.

The ration $\frac{C}{A}$ decreases with increasing k-point density for each pseudopotential. When the same k-mesh is used the ratio is very similar independent of used pseudopotential. The $36 \times 36 \times 19$ mesh reaches the DFT reference and the $12 \times 12 \times 12$ mesh is just 0.003 away from the ratio of the DFT reference.

### 3.5.4 Proportionality of k-meshes

As described in section 3.1.2 there is the argument that the amount of k-points along each reciprocal direction should be inversely proportional to related unitcell lengths. That would mean that for our system with $\frac{C}{A} = 1.624$ should have a ratio of $\frac{k_x}{k_z} = 1.624$. With 12 k-points in x-direction that would mean $k_z \approx 7.4$. The results of the relaxation calculations with k-meshes around these $12 \times 12 \times 7.4$ are shown in figure 3.5. There is always a trend with raising the amount of k-points in reciprocal z-direction. The lattice parameter $A$ increases with the amount of k-points while $C$ decreases. The ratio continues to drop with increasing amounts of k-points in reciprocal z-direction. With the exception of the PBE pseudopotentials without 'sol' in lattice parameter A,the $12 \times 12 \times 12$ is always the closest to the experimental reference.

### 3.5.5 Lattice parameters

The influence of different k-meshes on the length of the unitcell vectors is shown in the top and middle diagram in figure 3.5. It is visible that with higher k-point densities the values get closer to a fixed value which is dependent on the functional and has not to be the experimental reference. For the LDA functional and the highest k-point density it is still 0.05 Å and 0.08 Å off from the experimental reference for Aand C. For the PBE functional the DFT reference is reached, while PBEsol relaxes the lattice parameters 0.01 Å smaller than the experimental reference.

# 4 Discussion

The target was to find a set of simulation parameters for each pseudopotential which produces accurate results in manageable computation time. After that the pseudopotentials were compared to find the most suitable to calculate the starting wavefunction for a quantum algorithm.

## 4.1 Cutoff energies

The benchmark of the cutoff energies is the starting point of the benchmark of the simulation parameter and an important step with impact of the following steps.

The cutoff benchmark for the PBE PAW $2e^-$and PBEsol PAW $2e^-$pseudopotential is unambiguous. After a wavefunction cutoff of 80 Ry the total energy does not decrease any more and a plateau is reached. For the pseudopotentials which use 10 $e^-$ a higher cutoff is needed and even at a very high wavefunction cutoff of 100 Ry no plateau is reached. This implies that higher cutoffs could lead to a higher accuracy. The problem to consider is the increasing computational cost and time needed to calculate this many plane waves.

A wavefunction cutoff parameter of 100 Ry results in 6 times more plane waves then a wavefunction cutoff of 13 Ry. On the computer we used the single-point calculation with $E_{wfc} = 13\,\text{Ry}; E_\rho = 52\,\text{Ry}$ took 20-times less time then with $E_{wfc} = 100\,\text{Ry}; E_\rho = 400\,\text{Ry}$. This time difference is only an example and is dependent on lots of factors i. e. other people using the machine, amount of processors used and if GPU acceleration is used. That is the reason the computation time is not used quantitatively to compare the computational cost of different sets of simulation parameters.

## 4.2 Smearing

The smearing parameters are a tool to make simulations shorter or difficult simulation possible (see Baisuk et. al.[24]). The used value changes $E_{\text{tot}}$ and for more accurate results, the broadening parameter $E_{\text{degauss}}$should be reduced. The current system is simple enough that very little smearing is sufficient.

## 4.3 K-mesh benchmark

### 4.3.1 Amount of k-points

The amount of k-points along each reciprocal direction is a parameter which controls the density of k-points in this direction. It does influence the amount of calculated k-points, but is not the only influence. Due to symmetry of the crystal a lot of k-points are equivalent

to each other and have to be calculated only once. This reduces the amount of calculated k-points and the computation time. Furthermore it is the reason why there are different amounts of calculated k-points necessary for shifted and unshifted meshes to reach the same k-point density.

### 4.3.2 Position of k-meshes

The impact of shifting the k-mesh is due to the symmetry of the crystal. When coincidently the symmetry of the k-mesh aligns with the symmetry of the crystal it is possible that sampling of the first Brillouin-Zone is not optimal. It samples for example disproportional often minima. This is shown in figure 3.4, where at low amounts of k-points bigger deviations are visible. When more k-points are used both shifted and unshifted meshes give the same result because the first BZ is sampled more dense.

That shifted k-meshes need more calculated k-points is uncommon. Only in HCP cells the shift breaks the symmetry. Due to this symmetry break, a symmetrization is needed because the k-mesh should always have the same symmetry as the crystal. This symmetrization generates new k-points which increases the the amount of calculated k-points. This is also the explanation of the faster increase of calculated k-points in the shifted mesh.

## 4.4 Relaxation Calculations

### 4.4.1 Lattice parameters

With the same simulation parameters (same k-mesh and functional) the DFT reference values were reached. Unfortunately the calculated lattice parameters do not generally get closer to the experimental reference value with increasing k-point density. They seem to get closer to a fixed value, which is just near the experimental reference.

### 4.4.2 Proportionality of k-meshes

The results of the relaxation calculations shows that the shape of the calculated unitcell gets generally better with a higher k-point density in the z-direction independently of used pseudopotential. So a more unproportional k-mesh gets better results than a proportional. That does not mean that the guideline is wrong. It is more probable that a denser sampling of the BZ leads to better results. This is underlined by the calculations with the $36 \times 36 \times 19$ where a even better shape is reached with a proportional k-mesh.

### 4.4.3 Pseudopotentials

**Functionals** The functional of the pseudopotentials has the biggest impact on the relaxed lattice parameters. The LDA functional is less accurate than the GGAs, with values farther

away from the experimental reference. The LDA functional is less computational expensive than the GGA functionals.

The PBE functional estimates the unitcell lengths 0.01 Å to 0.03 Å to large, while the PBEsol functional estimates them 0.01 Å to 0.02 Å to small at the highest k-point density. The consequence is that the volume of the unitcell with the PBE functionals is bigger than the volume of the unitcells with the PBEsol functionals. It could be that in a smaller unitcell a hydrogen atom has a greater impact, than in a smaller one. We cannot decide which is a 'better' choice.

The differences in the shape of the unitcell is within a functional group bigger than the differences between the functionals are.

**Aktive electrons** The calculations with two active electrons per magnesium atom need smaller cutoffs and compute faster than the calculations with 10 active electrons. There is a small visible difference in lattice parameters and shape. This difference is in the magnitude of 0.001 Å and the significance is very small.

**Pseudopotential Type** The difference between the PAW and the US pseudopotentials is even smaller than the difference from different amounts of active electrons. This is reassuring because that implies that the same behaviour is modelled with different techniques and the same result is achieved.

# 5 Conclusion

The simulation parameters cutoff energies, smearing parameters and k-mesh were benchmarked for 7 pseudopotentials. The accuracy was tested with the lattice parameters as point of reference.

**System** The benchmark and accuracy test were done on a HCP magnesium crystal at 0 K with 2 atoms in the unitcell.

**Cutoff Energies** The $E_{wfc} = 100\,\mathrm{Ry}; E_{\rho} = 400\,\mathrm{Ry}$ cutoff parameters offer a good accuracy while being computational reasonable. For $2e^-$ pseudopotentials smaller cutoffs can be considered.

**Smearing** A modern smearing algorithm like Methfessel-Paxton is suitable for this magnesium system, but a smaller broadening coefficient $E_{\mathrm{degauss}}$than 0.03 Ry should be considered.

**K-mesh benchmark** The benchmark of the k-mesh judged by the total energy has two sides. It shows that the shifted k-mesh is more suitable for small amounts of k-points, where it calculates better results with a similar total amounts of k-points. At least a shifted $12 \times 12 \times 12$ k-mesh should be used, while the energy difference between a shifted and unshifted mesh vanishes at $18 \times 18 \times 18$. The second side is that the amount of calculated k-points increases faster with the shifted mesh than with the unshifted mesh. At high amounts of k-points along each axis the unshifted mesh calculates similar total energies with half the amount of calculated points.

**Pseudopotentials** The decision which pseudopotential to use is with the information of the benchmark and relaxation calculations not definite. Depending on the use case different choices can be suitable. The GGA functionals have a better accuracy than the LDA functional.

**Level of theory** A sufficient level of theory for each pseudopotential was found. The results of a calculation with the benchmarked simulation parameters could be used for future calculations. The accuracy of the lattice parameter is known.

**'Best' Pseudopotential** The decision which pseudopotential to use is dependent not only on the accuracy, but also for what the simulation will be used. When the wavefunction of

more than 2 electrons per magnesium atom is needed, a pseudopotential with 10 electrons should be used. A decision between the PBE and PBEsol functional is difficult. When possible both should be tested. With the results of the benchmark of this thesis no decision can be made. Only with further requirements or information one could be better than the other. The PAW pseudopotentials with the same amount of active electrons took insignificant less time then the US pseudopotentials. For this observable no decision can be made.

In the next thesis these different pseudopotentials will be tested in the quantum computing workflow to compare them further.

# References


[1] Nandhini S, Harpreet Singh and Akash U N. An extensive review on quantum computers. *Advances in Engineering Software* 174, 2022, p. 103337.

[2] Sandeep Kumar Dwivedi and Manish Vishwakarma. Hydrogen embrittlement in different materials: A review. *International Journal of Hydrogen Energy* 43.46, 2018, pp. 21603–21616.

[3] Zhao, H., Chakraborty, P., Ponge, D., Hickel, T., Sun, B., Wu, C.-H., Gault, B. and Raabe, D. Hydrogen trapping and embrittlement in high-strength Al alloys. *Nature* 602.7897, 2022, pp. 437–441.

[4] Schrödinger, E. An Undulatory Theory of the Mechanics of Atoms and Molecules. *Phys. Rev.* 28.6, 1926, pp. 1049–1070.

[5] Perdew, J. P. Climbing the ladder of density functional approximations. *MRS Bulletin* 38.9, 2013, pp. 743–750.

[6] Fock, V. Näherungsmethode zur Lösung des quantenmechanischen Mehrkörperproblems. *Zeitschrift für Physik* 61.1, 1930, pp. 126–148.

[7] Vogiatzis, K. D., Ma, D., Olsen, J., Gagliardi, L. and Jong, W. A. de. Pushing configuration-interaction to the limit: Towards massively parallel MCSCF calculations. *The Journal of chemical physics* 147.18, 2017, p. 184111.

[8] Giannozzi, P. et al. QUANTUM ESPRESSO: a modular and open-source software project for quantum simulations of materials. *Journal of Physics: Condensed Matter* 21.39, 2009, 395502 (19pp).

[9] Giannozzi, P. et al. Advanced capabilities for materials modelling with QUANTUM ESPRESSO. *Journal of Physics: Condensed Matter* 29.46, 2017, p. 465901.

[10] Giannozzi, P. et al. Quantum ESPRESSO toward the exascale. *The Journal of chemical physics* 152.15, 2020, p. 154105.

[11] Koch, W. and Holthausen, M. C. *A Chemist's Guide to Density Functional Theory.*

[12] Worch, H., Pompe, W. and Schatt, W. *Werkstoffwissenschaft.* 10., vollst. überarb. Aufl. Weinheim: Wiley-VCH, 2011.

[13] Meyer, B. The pseudopotential plane wave approach. *NIC Series* 31, 2006, p. 71.

[14] Bloch, F. Über die Quantenmechanik der Elektronen in Kristallgittern. *Zeitschrift für Physik* 52.7, 1929, pp. 555–600.

[15] Gonze, X. et al. The Abinit project: Impact, environment and recent developments. *Comput. Phys. Commun.* 248, 2020, p. 107042.

[16] Frisch, M. J. et al. *Gaussian˜16 Revision C.01*. 2016.

[17] Kresse, G. and Furthmüller, J. Efficient iterative schemes for ab initio total-energy calculations using a plane-wave basis set. *Phys. Rev. B* 54.16, 1996, pp. 11169–11186.

[18] Monkhorst, H. J. and Pack, J. D. Special points for Brillouin-zone integrations. *Phys. Rev. B* 13.12, 1976, pp. 5188–5192.

[19] Yin, B., Wu, Z. and Curtin, W. A. Comprehensive first-principles study of stable stacking faults in hcp metals. *Acta Materialia* 123, 2017, pp. 223–234.

[20] Barrett, C. S., Massalski, T. B., Barrett, C. and Massalski, T. *Structure of metals Crystallographic methods, principles, and data: International series on materials science and technology ; 35*. 3. rev. ed. Oxford [u.a.]: Pergamon Pr, 1980.

[21] Pople, J. A. Nobel Lecture: Quantum chemical models. *Reviews of Modern Physics* 71.5, 1999, pp. 1267–1274.

[22] Prandini, G., Marrazzo, A., Castelli, I. E., Mounet, N. and Marzari, N. Precision and efficiency in solid-state pseudopotential calculations. *npj Computational Materials* 4.1, 2018, p. 72.

[23] Marzari, N. Ab-initio molecular dynamics for metallic systems, 1996,

[24] Vladimir A. Basiuk, Oleg V. Prezhdo and Elena V. Basiuk. Thermal smearing in DFT calculations: How small is really small? A case of La and Lu atoms adsorbed on graphene. *Materials Today Communications* 25, 2020, p. 101595.

# A Appendix

## A.1 Cutoff benchmark

Cutoff energy Benchmark: The total energy $E_{\text{tot}}$ of a two magnesium atoms system is depicted over the charge density cutoff $E_\rho$. The single-point calculations were done with with following parameters: $A = 3.2\,\text{nm}; C = 5.226\,\text{nm}$; Methfessel-Paxton smearing with $E_{\text{degauss}}$= 0.03 Ry;8x8x8 k-mesh and the in the title given pseudopotential

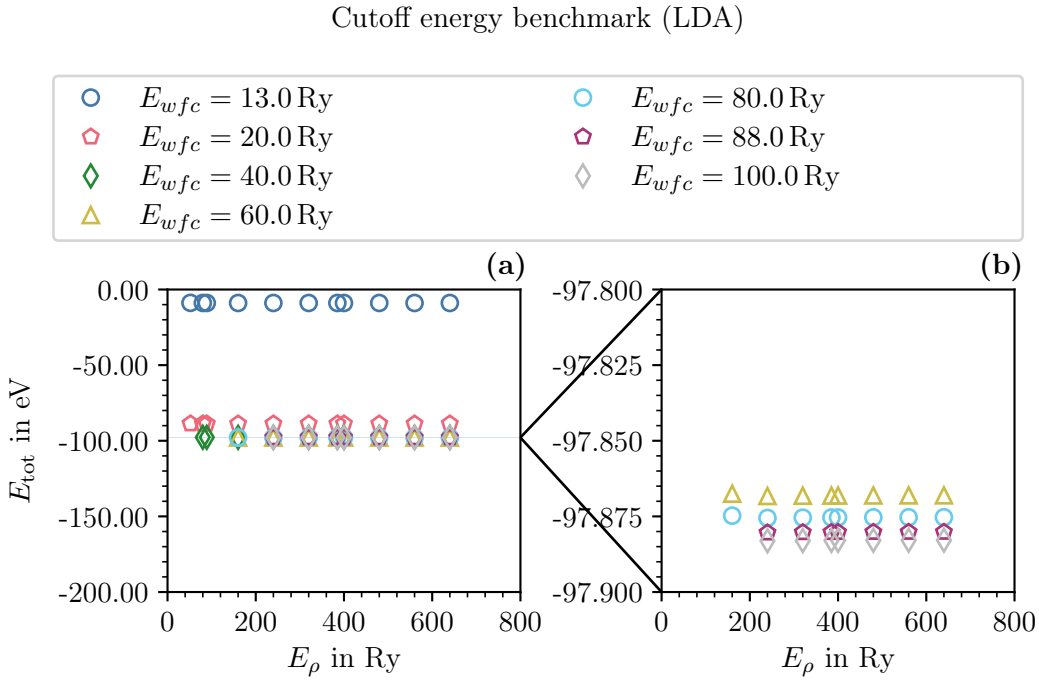


Figure A.1: Cutoff energy benchmark(LDA), $E_{\text{tot}}$ is shifted by $-3700\,\text{eV}$.

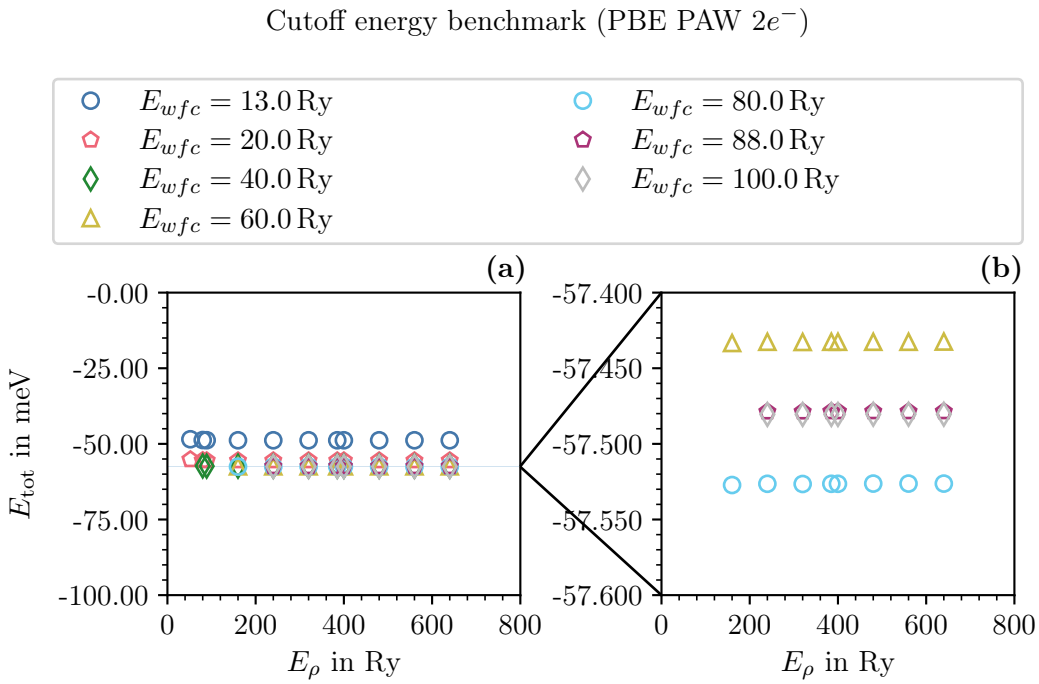


Figure A.2: Cutoff energy benchmark(PBE PAW $2e^-$), $E_{\mathrm{tot}}$ is shifted by $-914.7\,\mathrm{eV}$.

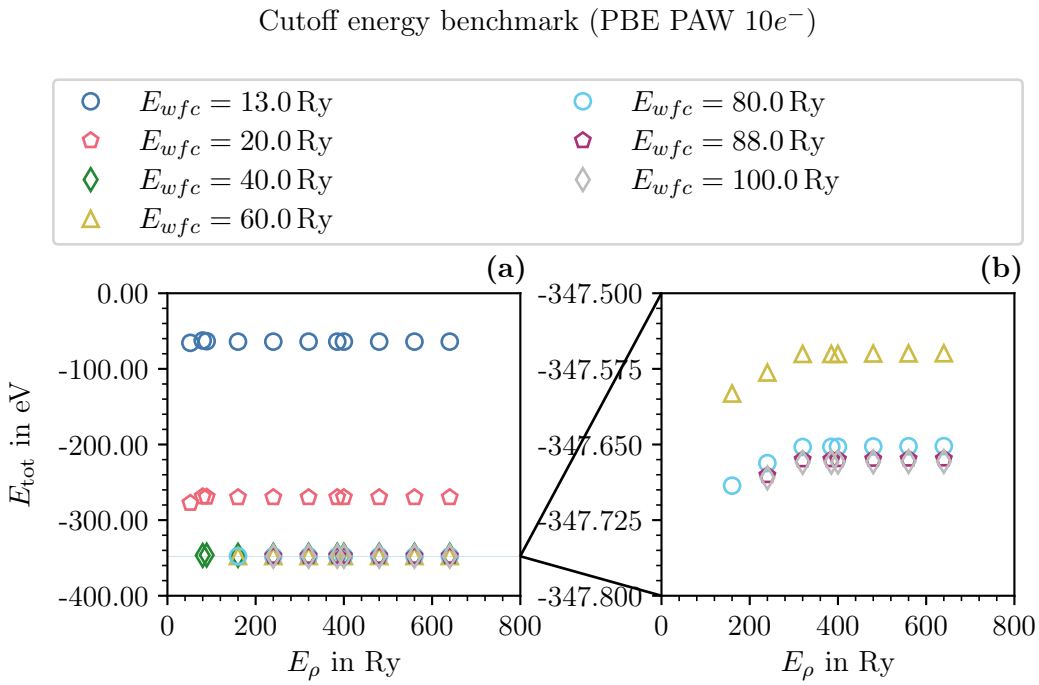


Figure A.3: Cutoff energy benchmark(PBE PAW $10e^-$), $E_{\mathrm{tot}}$ is shifted by $-3500\,\mathrm{eV}$.

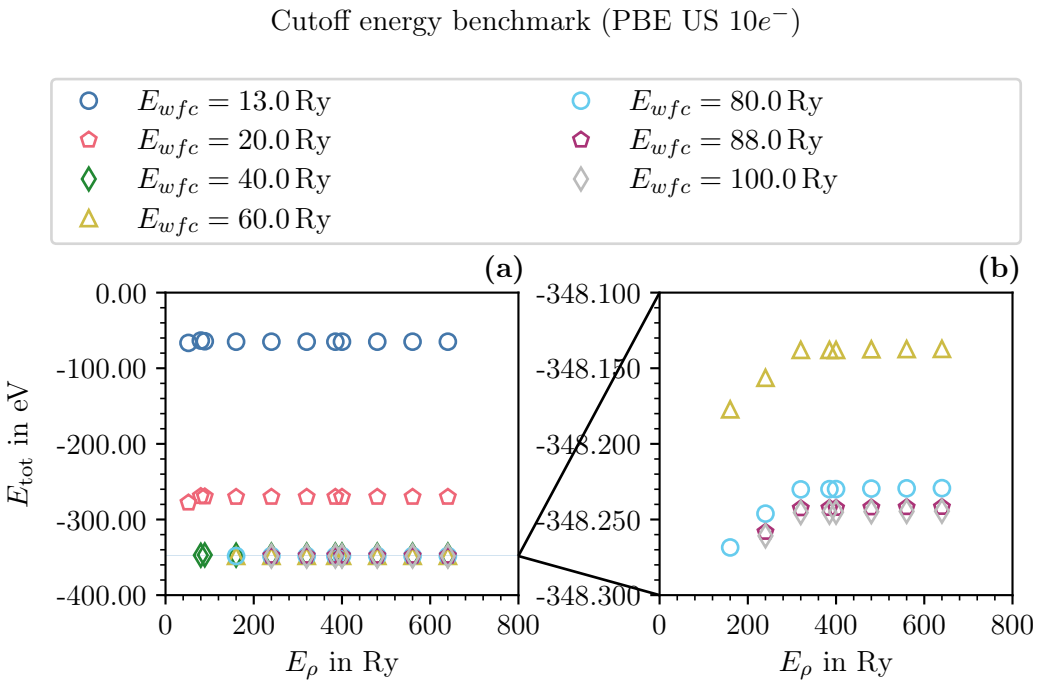


Figure A.4: Cutoff energy benchmark(PBE US $10e^-$), $E_{\mathrm{tot}}$ is shifted by $-3100\,\mathrm{eV}$.

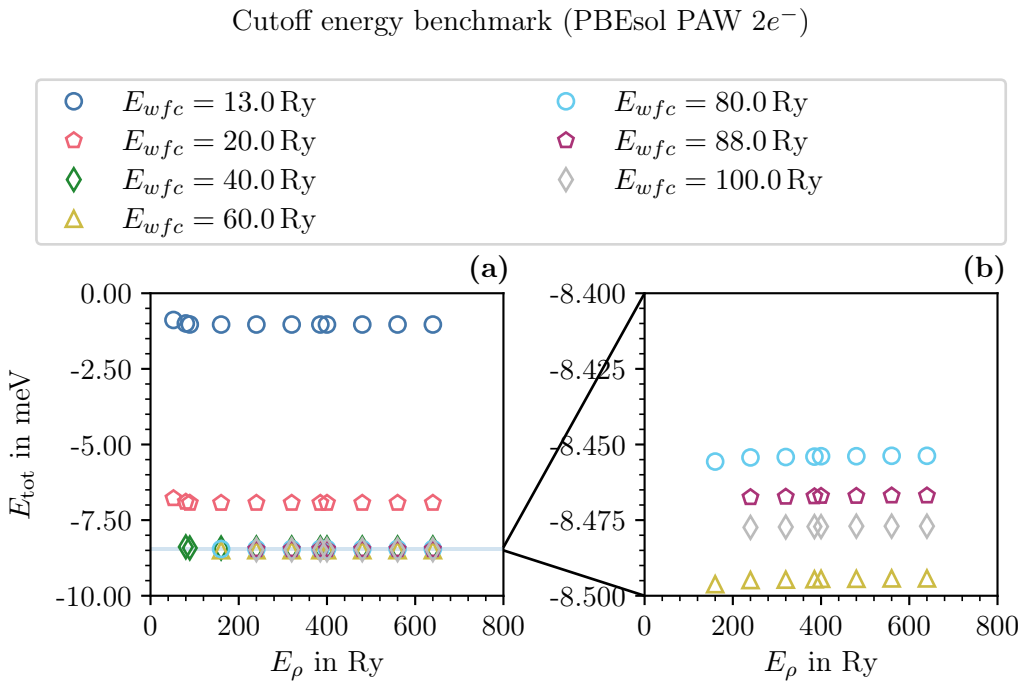


Figure A.5: Cutoff energy benchmark(PBEsol PAW $2e^-$), $E_{\mathrm{tot}}$ is shifted by $-890.34\,\mathrm{eV}$.

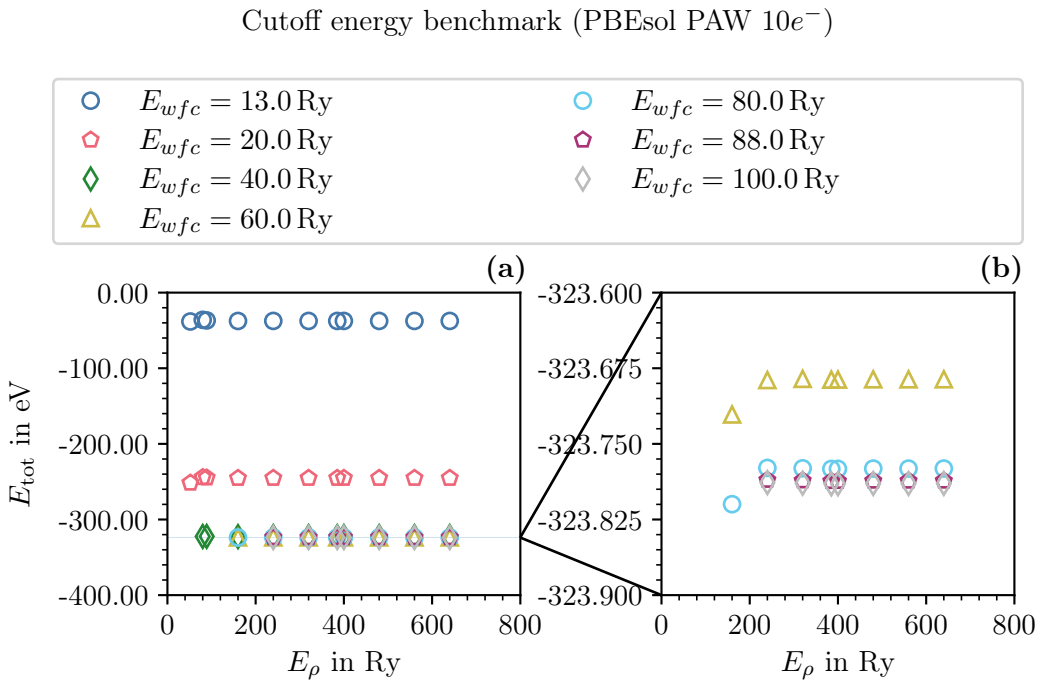


Figure A.6: Cutoff energy benchmark(PBEsol PAW $10e^-$), $E_{\mathrm{tot}}$ is shifted by $-3500\,\mathrm{eV}$.

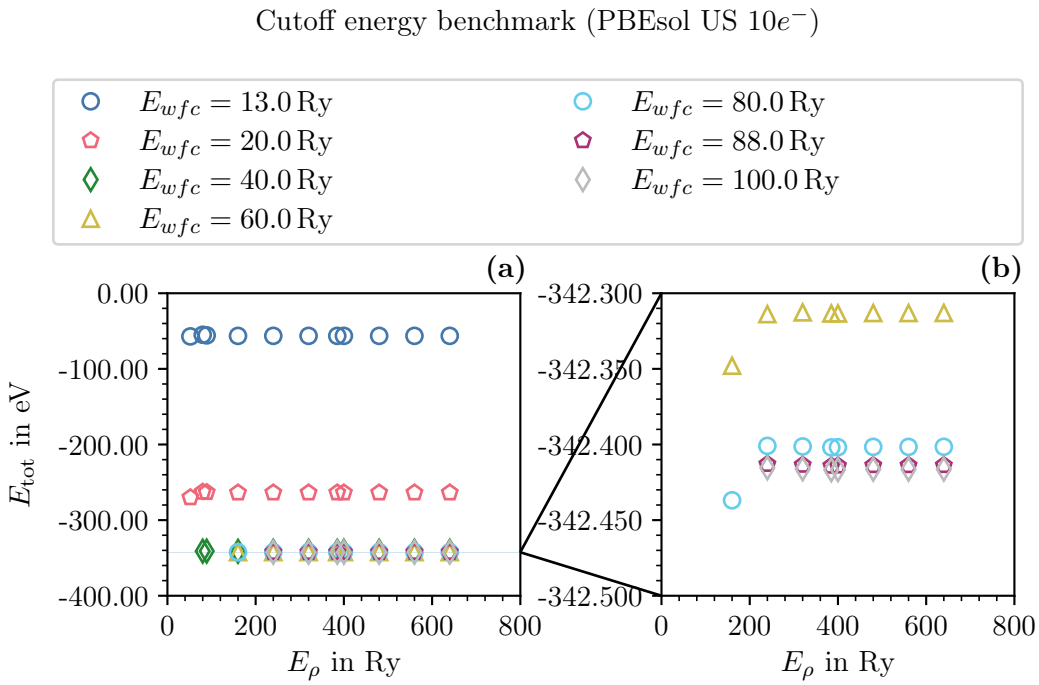


Figure A.7: Cutoff energy benchmark(PBEsol US $10e^-$), $E_{\mathrm{tot}}$ is shifted by $-3100\,\mathrm{eV}$.

## A.2 Smearing benchmark

Smearing Benchmark: The total energy $E_{\text{tot}}$ of a two magnesium atoms system is depicted over $E_{\text{degauss}}$. The single-point calculations were done with with following parameters: $A = 3.2\,\text{nm}; C = 5.226\,\text{nm}; E_{wfc} = 100\,\text{Ry}; E_{\rho} = 400\,\text{Ry}$; $8 \times 8 \times 8$ shifted k-mesh, in the title given pseudopotential

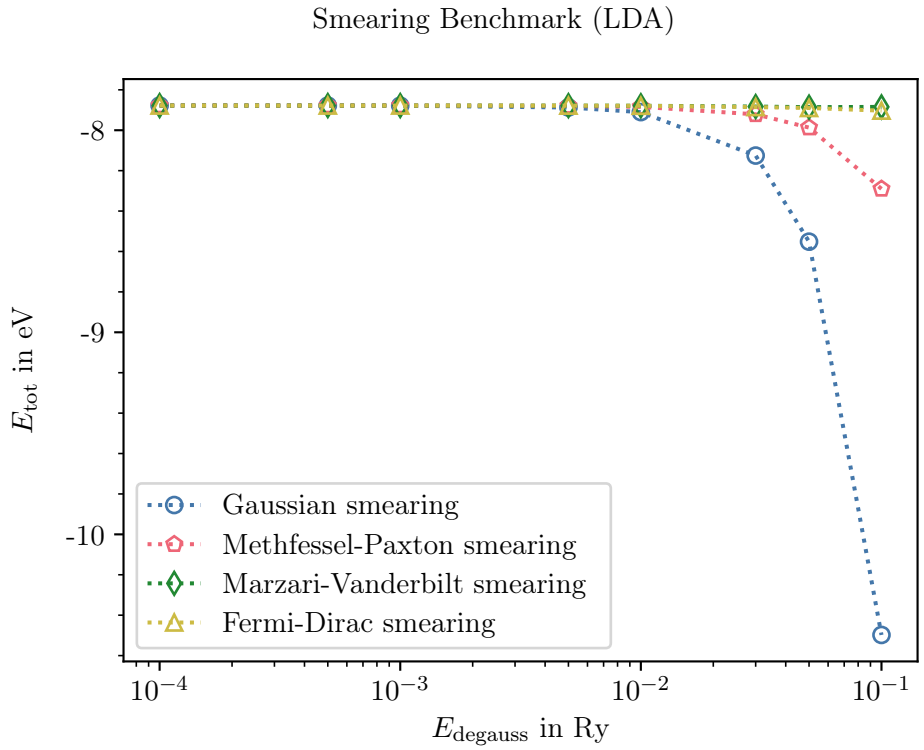


Figure A.8: Smearing energy benchmark(LDA), $E_{\text{tot}}$ is shifted by $-3790\,\text{eV}$.

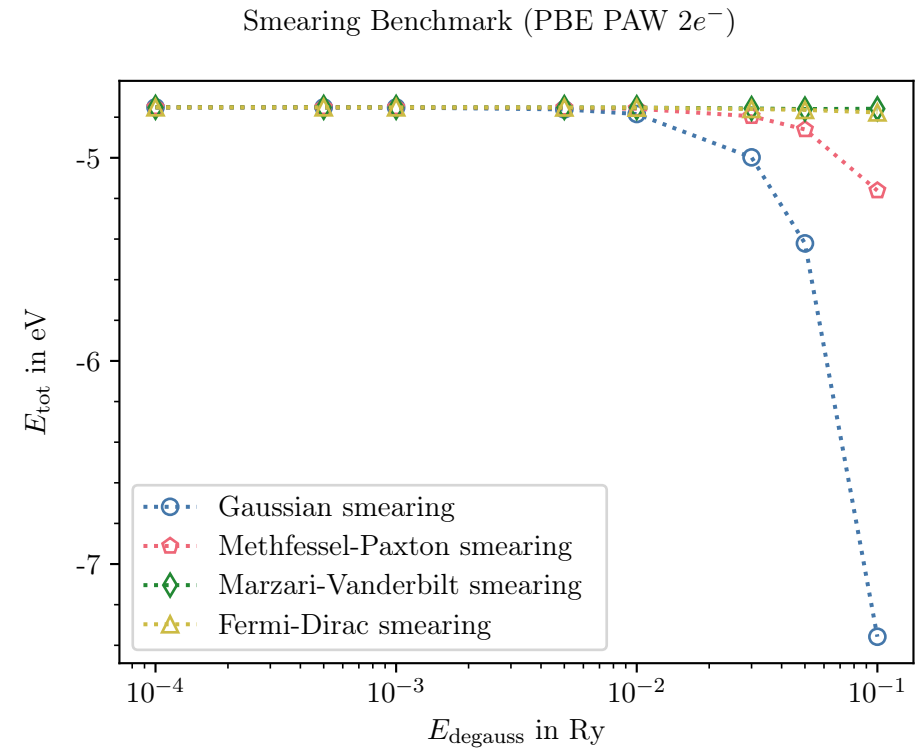


Figure A.9: Smearing energy benchmark(PBE PAW $2e^-$), $E_{\text{tot}}$ is shifted by $-910\,\text{eV}$.

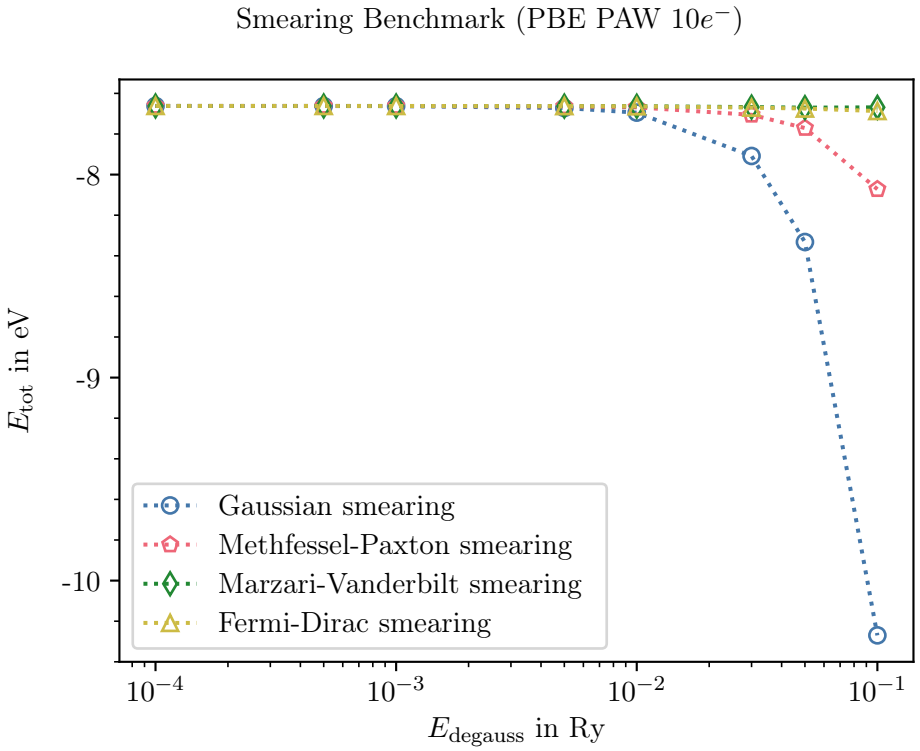


Figure A.10: Smearing energy benchmark(PBE PAW $10e^-$), $E_{\text{tot}}$ is shifted by $-3840\,\text{eV}$.

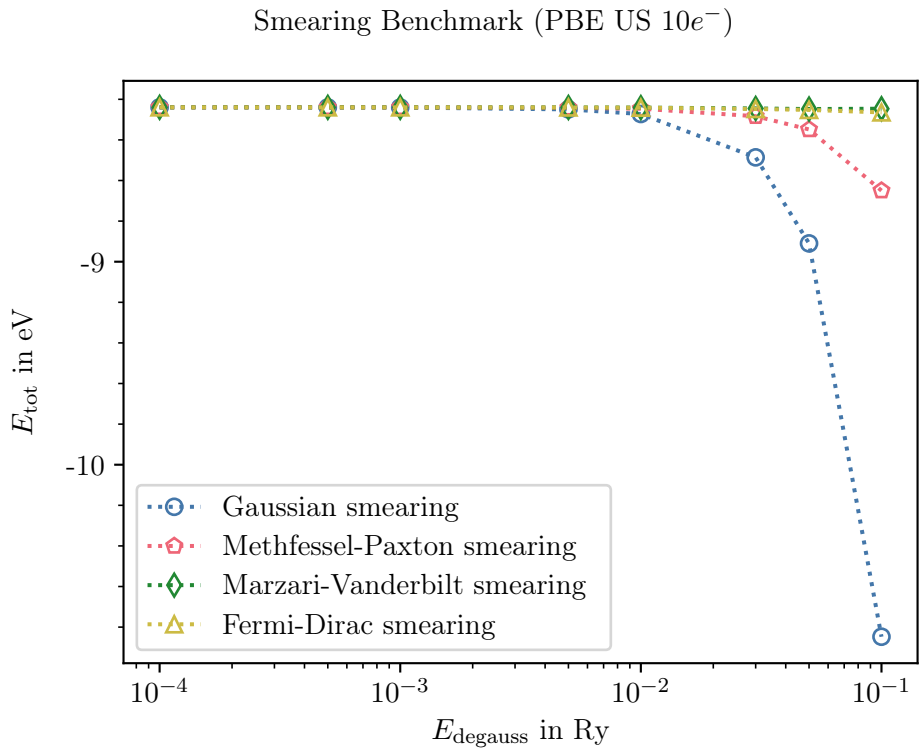


Figure A.11: Smearing energy benchmark(PBE US $10e^-$), $E_{\text{tot}}$ is shifted by $-3440\,\text{eV}$.

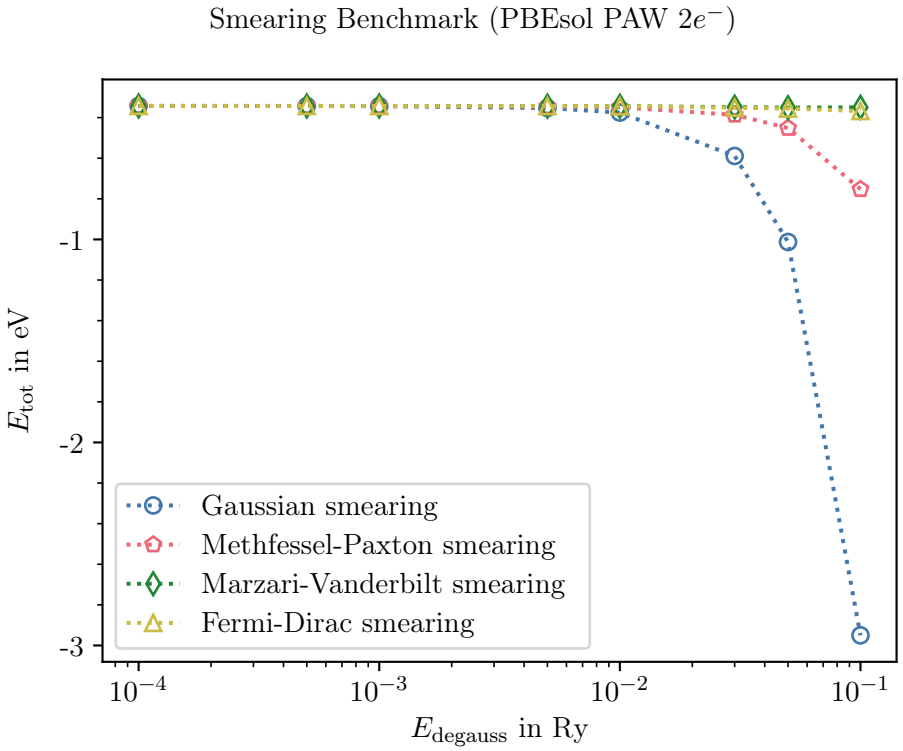


Figure A.12: Smearing energy benchmark(PBEsol PAW $2e^-$), $E_{\text{tot}}$ is shifted by $-890\,\text{eV}$.

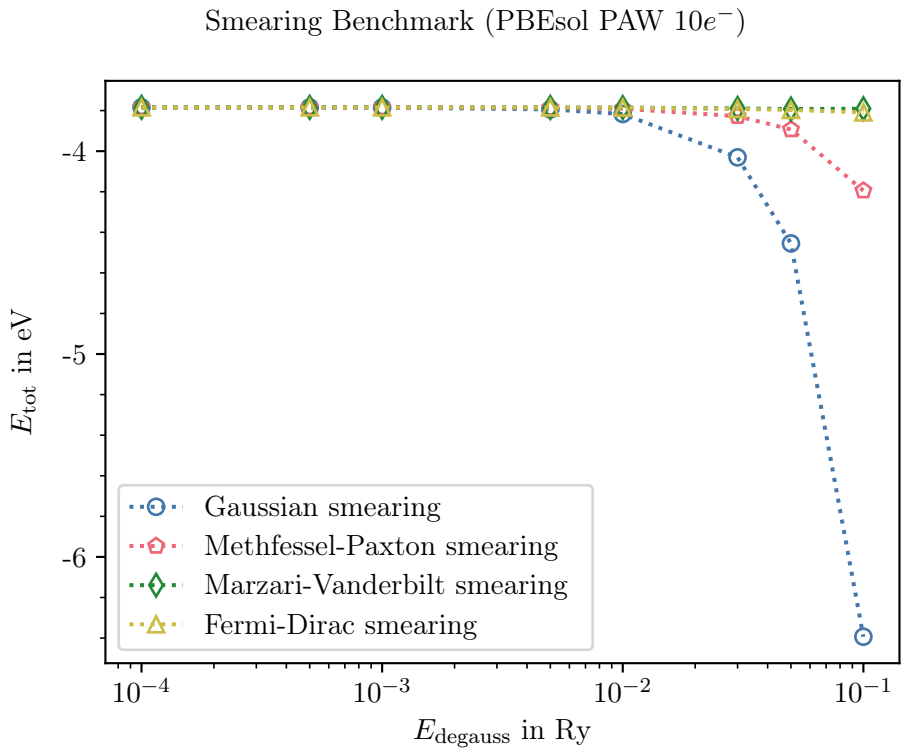


Figure A.13: Smearing energy benchmark(PBEsol PAW $10e^-$), $E_{\text{tot}}$ is shifted by $-3820\,\text{eV}$.

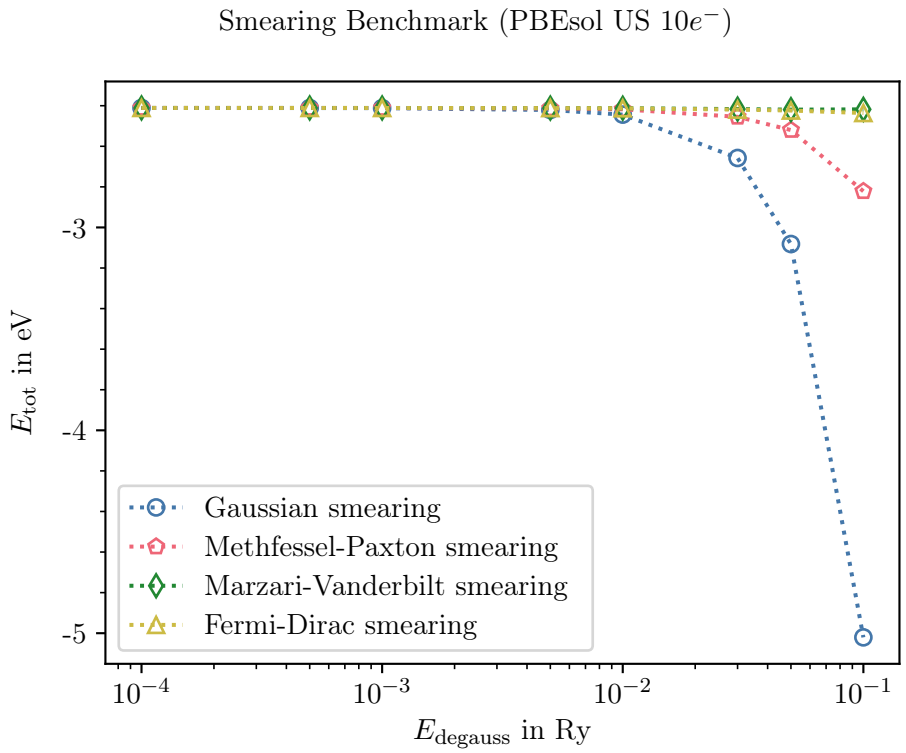


Figure A.14: Smearing energy benchmark(PBEsol US $10e^-$), $E_{\text{tot}}$ is shifted by $-3440\,\text{eV}$.

## A.3 k-point benchmark

k-mesh Benchmark: The total energy $E_{\text{tot}}$ of a two magnesium atoms system and the total amount of calculated k-points is depicted over the used k-mesh in the form of $k_x \times k_y \times k_z$. The single-point calculations were done with with following parameters: $A = 3.2\,\text{nm}; C = 5.226\,\text{nm}$; $E_{wfc} = 100\,\text{Ry}$; $E_\rho = 400\,\text{Ry}$; Methfessel-Paxton smearing with $degauss = 0.03\,\text{Ry}$; in the title given pseudopotential

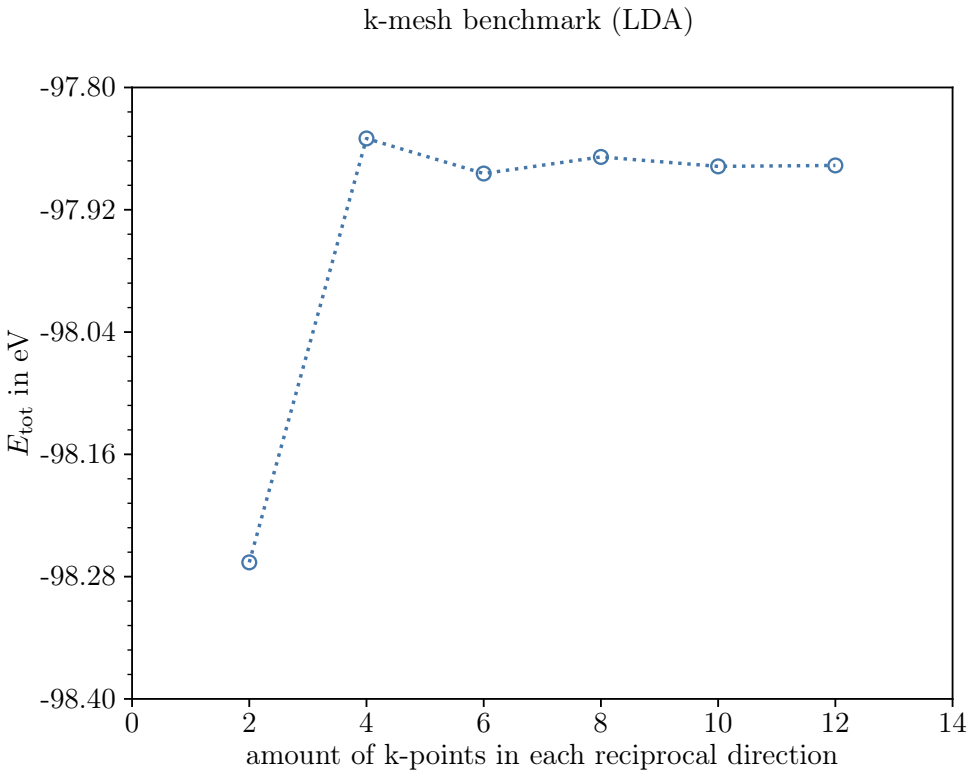


Figure A.15: k-point energy benchmark(LDA), $E_{\text{tot}}$ is shifted by $-3700\,\text{eV}$.

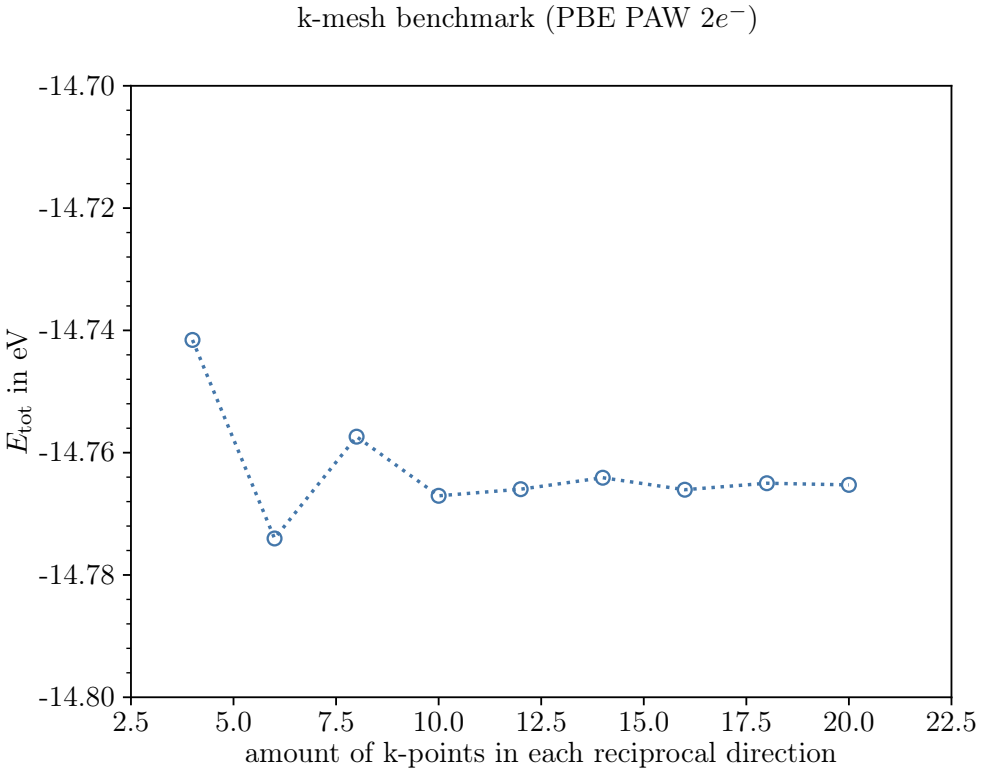


Figure A.16: k-point energy benchmark(PBE PAW $2e^-$), $E_{\text{tot}}$ is shifted by $-900\,\text{eV}$.

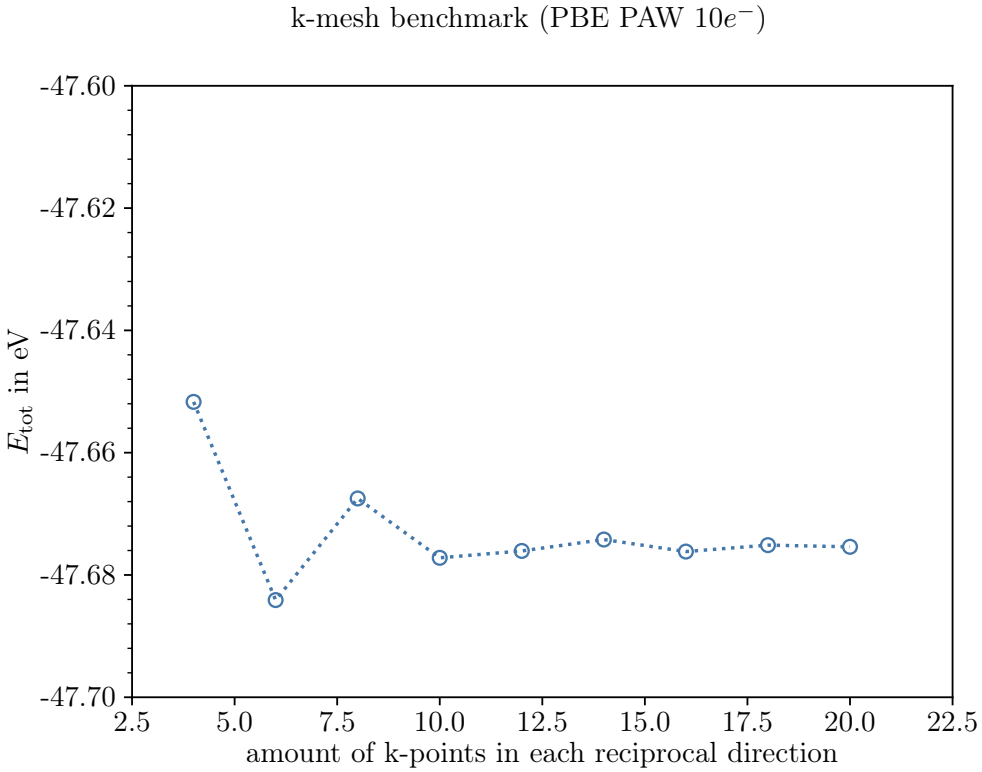


Figure A.17: k-point energy benchmark(PBE PAW $10e^-$), $E_{\text{tot}}$ is shifted by $-3800\,\text{eV}$.

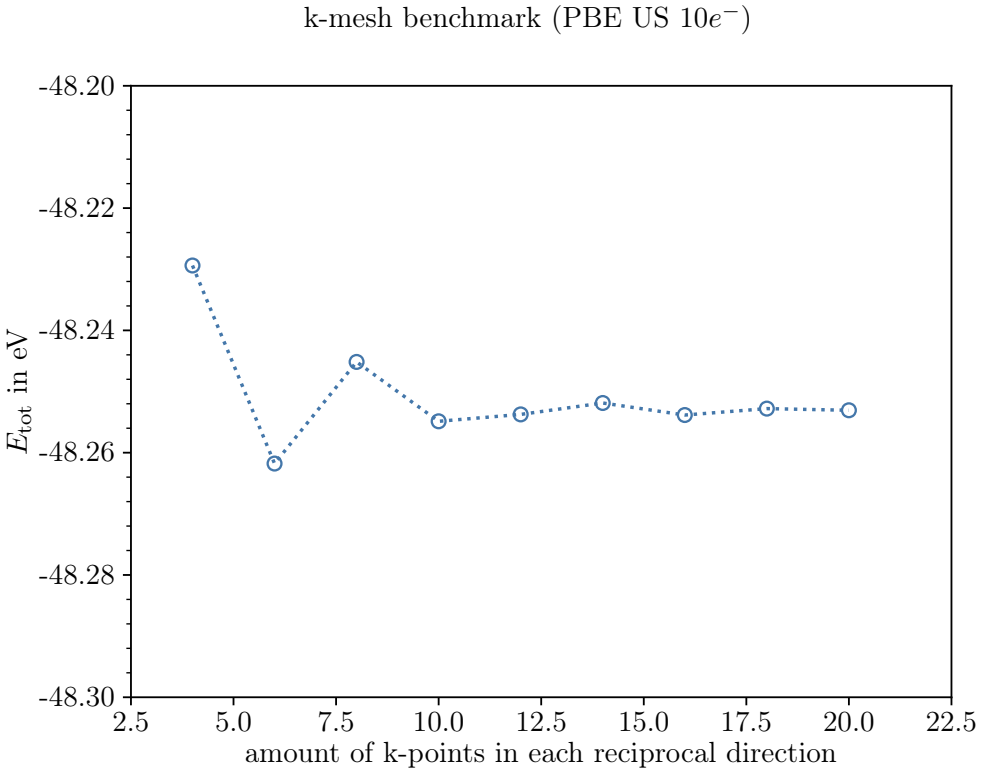


Figure A.18: k-point energy benchmark(PBE US $10e^-$), $E_{\text{tot}}$ is shifted by $-3400\,\text{eV}$.

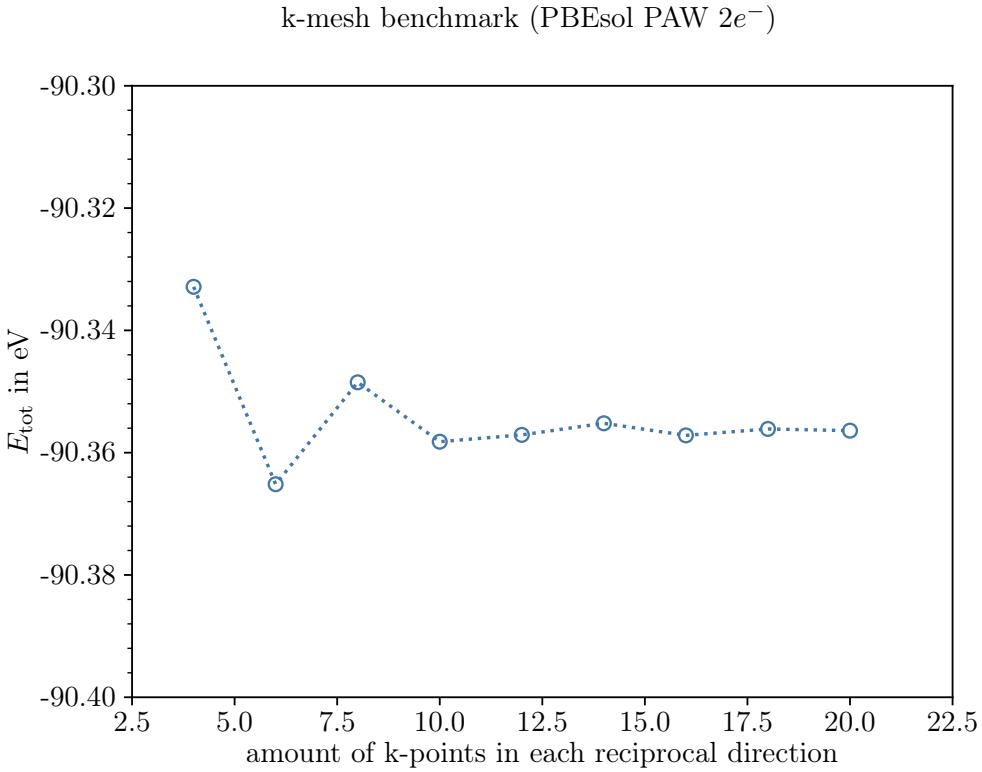


Figure A.19: k-point energy benchmark(PBEsol PAW $2e^-$), $E_{\text{tot}}$ is shifted by $-800\,\text{eV}$.

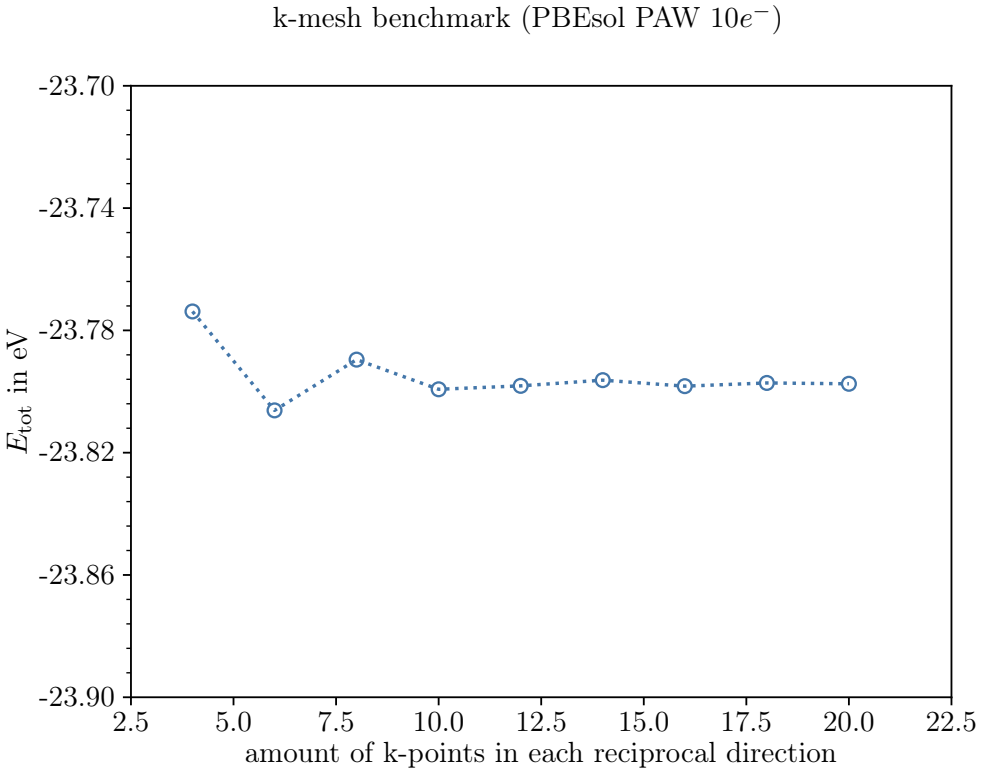


Figure A.20: k-point energy benchmark(PBEsol PAW $10e^-$), $E_{\text{tot}}$ is shifted by $-3800\,\text{eV}$.

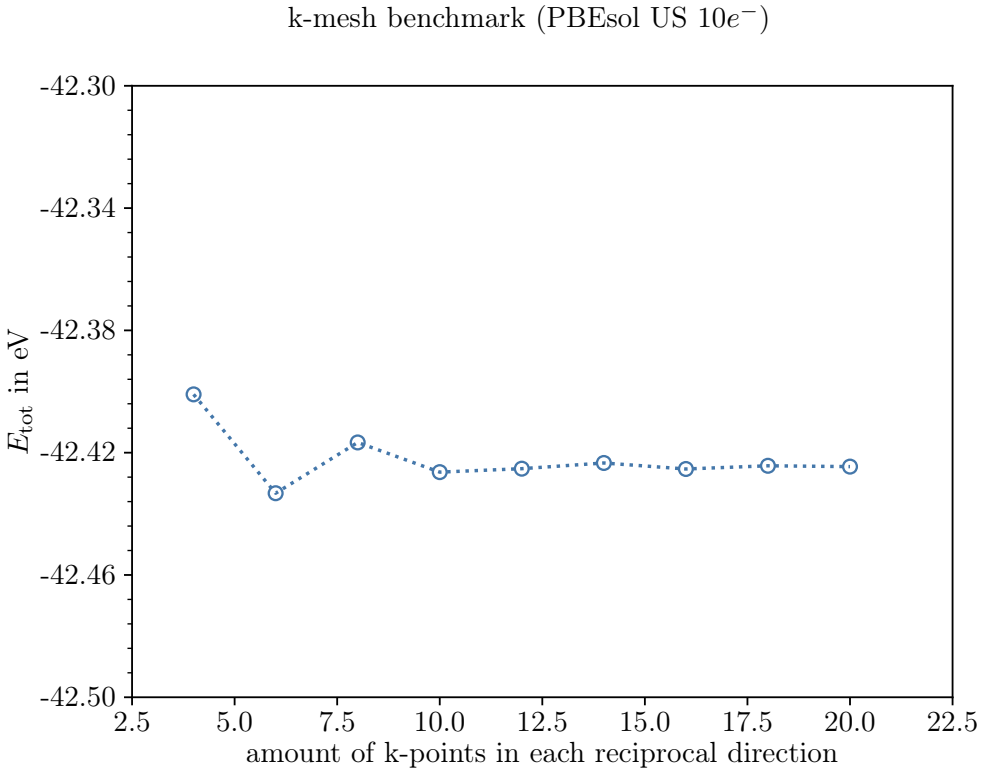


Figure A.21: k-point energy benchmark(PBEsol US $10e^-$), $E_{tot}$ is shifted by $-3400\,\text{eV}$.

# Statement of Originality

This thesis has been performed independently with support by the candidate's supervisors. It contains no material that has been accepted for the award of a degree in this or any other university. To the best of the candidate's knowledge and belief, this thesis contains no material previously published or written by another person except where due reference is made.

Köln, 31. March 2024

Alexander Rehn